5-2015

MICRORNA-200 REGULATES ECM-DEPENDENT β1-INTEGRIN/ FAK SIGNALING AND CANCER CELL INVASION

Christin Ungewiss

MICRORNA-200 REGULATES ECM-DEPENDENT β1-INTEGRIN/FAK SIGNALING AND CANCER CELL INVASION THROUGH CRKL

by

Christin Ungewiss, B.S.

APPROVED:

_____
Advisory Professor
Don L. Gibbons, M.D., Ph.D.

_____
Andrew B. Gladden, Ph.D.

_____
Faye M. Johnson, M.D., Ph.D.

_____
Jonathan M. Kurie, M.D.

_____
Yang Xia, M.D., Ph.D.

APPROVED:

_____
Dean, The University of Texas
Graduate School of Biomedical Sciences at Houston

MICRORNA-200 REGULATES ECM-DEPENDENT β1-INTEGRIN/FAK SIGNALING AND CANCER CELL INVASION THROUGH CRKL

A

DISSERTATION

Presented to the Faculty of
The University of Texas
Health Science Center at Houston
and
The University of Texas
MD Anderson Cancer Center
Graduate School of Biomedical Sciences
in Partial Fulfillment

of the Requirements

for the Degree of

DOCTOR OF PHILOSOPHY

by

Christin Ungewiss, B.S.
Houston, Texas

May 2015

Dedication

I dedicate this thesis to my wonderful husband Ronny without whom this journey would have been impossible. He was the driving force for us to make the big move from Germany to Houston, TX in order for me to attend graduate school. My husband has been my strongest support throughout the past years, he was always encouraging, listened to me at all times and put up with me during the most stressful times. Thank you for always being there for me!

I would also like to thank my parents and grandparents who taught me to never give up and work towards your goal without ever losing sight of it. All of them have been a tremendous support for me during my undergraduate and graduate studies. I'm truly blessed to always have received all the love and support one could possibly need in life.

Acknowledgments

I would like to thank my thesis advisor, Don Gibbons, for all his support throughout the last 4 years. He has been the best mentor a student can ever ask for. I appreciate all the time he took talking about experiments, thoughtfully discussing data, his continuous encouragement and his never-ending optimism. His door was always open whenever I needed someone to talk to, be it professional or personal. He taught me to be more confident during presentations, to critically think about science and to appreciate negative results, as they often hide unexpected surprises. I want to thank him for the many opportunities he gave me to talk about my science while at conferences, for patiently teaching me to improve my scientific writing, for appreciating my scientific opinions and for making me an overall better scientist. His positive attitude and appreciation towards his lab members are a unique characteristic, which I will definitely miss.

Next, I would like to thank my committee members Drs. Andrew Gladden, Faye Johnson, Jonathan Kurie and Yang Xia for all the time they took attending my committee meetings and personal meetings. I am very thankful for all the constructive feedback I have received over the past years, helping me to guide my project the right way and believing in my science. I would like to especially thank Dr. Jonathan Kurie, in whose lab I did an internship before I joined GSBS, and who was a tremendous help and encouragement to make me pursue a Ph.D. here at GSBS. Without him I would not be where I am today.

A big thank you goes to all the lab members of the Gibbons' lab, former and current ones, for all their help throughout my thesis work. Especially Dr. Jonathon Roybal has always been there for me, as a co-worker but most importantly as a friend. He always found the right words of encouragement in times of desperation and told me that things will always work out. Without him, the past years would have been a lot less fun and harder to focus on that light at the end of the tunnel.

And finally, I would like to thank my husband and family, parents and grandpa, for always supporting me and believing in me. Throughout all those years they showed interest in my research and were there for me when I needed someone to just listen. Thank you to everyone for supporting me during this journey!!!

MICRORNA-200 REGULATES ECM-DEPENDENT β1-INTEGRIN/FAK SIGNALING AND CANCER CELL INVASION THROUGH CRKL

Christin Ungewiss, B.S.

Advisory Professor: Don L. Gibbons, M.D., Ph.D.

The microRNA-200 family is known to be a master regulator of the epithelial-to-mesenchymal transition, partially through its double-negative feedback loop with the transcriptional repressor Zeb1, yet the mechanisms on how miR-200 controls the invasive phenotype are not fully understood. Recent studies have shown that the miR-200/Zeb1 axis regulates cell-cell and cell-matrix interactions, but it has also been demonstrated that cell-intrinsic changes are insufficient to drive cancer cell invasion, leading us to focus on specific cell-matrix interactions required to activate tumor cell invasion and metastases. We have shown through 3D studies that the Integrin β1-collagen I contact is critical in mediating the invasive phenotype in cells with miR-200 loss or Zeb1 overexpression. Furthermore, those genetic changes enhanced the cells responsiveness to the ECM through the FAK/Src pathway. The importance of this pathway in our Kras and p53 mouse model and in human lung cancer cell lines was further studied using pharmacological inhibitors and an shRNA-based knockdown approach, which exhibited a significant suppression of migration and invasion in Boyden chambers and 3D invasion assays. Furthermore, pharmacological inhibition of Src prevented distant metastases *in vivo*. We found

that miR-200 regulates the activation of the FAK/Src pathway through direct targeting of CRKL, an integrin adaptor molecule. Our studies suggest that CRKL is critical in enhancing the outside-in signaling through ltgβ1 but also involved in the inside-out signaling by maintaining the cell-matrix contact required for continuous cell invasion. Those findings highlight the importance of the ECM composition, in addition to cell-intrinsic changes, that regulate the activation of intracellular signaling pathways required for tumor cell invasion and metastases that allow for targeting at multiple levels.

Table of Contents

List of Illustrations

List of Tables

Abbreviations

3’-UTR	three prime untranslated region
bp	base pairs
CDH1	Cadherin 1, E-cadherin
CDH2	Cadherin 2, N-cadherin
CML	chronic myeloid leukemia
Coll	Collagen Type I
CSK	c-Src tyrosine kinase
Cttn	Cortactin
DA	dominant active
DAPI	4',6-diamidino-2-phenylindole
Das	Dasatinib
db mut	double mutant
DMSO	Dimethyl sulfoxide
DN	dominant negative
Dox	Doxycycline
ECM	extracellular matrix

EDTA	ethylenediaminetetraacetic acid
EMT	epithelial-to-mesenchymal transition
F-actin	filamentous actin
FAK	focal adhesion kinase
FN	Fibronectin
GFP	green fluorescent protein
IACUC	institutional animal care and use committee
IgG	Immunoglobulin G
IgM	Immunoglobulin M
Ima	Imatinib
Itgβ	Integrin beta
KD	knockdown
KP	$Kras^{G12D}$ $p53^{R172H\Delta G}$
LN	lymph node
MET	mesenchymal-to-epithelial transition
MG	Matrigel
miR	microRNA

mRNA	messenger ribonucleic acid
NSCLC	non-small cell lung cancer
Pax	Paxillin
PBS	Phosphate buffered saline
pre-miR	pre-microRNA
qPCR	quantitative real-time polymerase chain reaction
RIPA buffer	radioimmunoprecipitation assay buffer
RT-PCR	Real Time Polymerase Chain Reaction
scr	scramble control
SFK	Src-family kinases
shRNA	short hairpin RNA
siRNA	small interfering RNA
SQ	subcutaneous
TBST	Tris-Buffered Saline and Tween 20
TGFβ	transforming growth factor beta
unt	untreated
wt	wild type

Chapter 1

Introduction

Lung cancer

Lung cancer is a heterogeneous disease that is divided into two main types, non-small cell lung cancer (NSCLC, ~ 80-85 %) and small cell lung cancer (~15-20 %). NSCLC can be further classified into adenocarcinoma, squamous carcinoma, large cell carcinoma, bronchoalveolar lung cancer and mixed types [1]. Lung cancer is listed as the second cancer type in the number of new estimated cases in both men and women and the leading cause of all cancer-related deaths, accounting for 160,000 deaths per year in the United States. This can be explained by the fact that almost 2/3 of the patients when they first present already have metastatic disease, which has a 5 year survival rate of less than 5 % and has not changed over the past decades [2]. Understanding the molecular mechanisms underlying metastasis is therefore crucial in developing better treatment strategies. In order to study metastasis, a mouse model was previously developed in which mice carrying a somatic activation of the $Kras^{G12D}$ allele will develop lung adenocarcinoma but not metastasize. Introduction of the mutant p53 allele ($p53^{R172H\Delta G}$), commonly found in Li-Fraumeni syndrome, into those mice causes the development of atypical adenomatous hyperplasia, adenomas and adenocarcinomas. The lung adenocarcinomas found in this model are highly metastatic, with metastases found at sites commonly seen in NSCLC patients. Transcriptional profiling of the tumors derived from this mouse model revealed a metastases signature that correlated with a subset of NSCLC patients with poor prognosis [3, 4].

Metastases and epithelial-to-mesenchymal transition

Metastasis is a complex, multi-step process, in which cancer cells disseminate from the primary tumor by invasion into the surrounding ECM, intravasate, are transported through the blood circulation and extravasate from the blood vessels at distant organs, where they can form secondary tumors through establishment of micro-metastases, allowing for a rapid spread of cancer cells [5]. It is thought that cancer cells typically undergo an epithelial-to-mesenchymal transition (EMT) in order to gain migratory and invasive properties. Epithelial cells, found in the primary tumor, are characterized by tight junctions and an apical-basal polarity, and their cobble-stone like organization. Mesenchymal cells show an increased expression of mesenchymal markers, such as N-cadherin, ZEB1/2 and vimentin, allowing for increased motility through a decrease in cell-cell contact, displayed by their scattered, fibroblast-like appearance [6-8]. The transcriptional repressors ZEB1 and ZEB2 have been shown to regulate EMT by suppressing the transcription of epithelial markers such as E-cadherin by binding to the E-boxes in the promoter region [9]. Furthermore, the invasive phenotype that tumor cells acquire upon metastasis is characterized by a reorganization of the actin cytoskeleton to drive the leading edge of the cell forward and to recruit actin-associated proteins and metallo-proteases necessary for the degradation of the extracellular matrix (ECM).

miR-200/ZEB1 axis and the extracellular matrix

MicroRNAs are small non-coding RNAs that bind to the 3’ untranslated region (3’UTR) of genes, thereby regulating their expression by targeting them for degradation or repression of translation [10]. The miR-200 family consists of five

family members, 200a/b/c, 141 and 429, located on two different genomic loci: 200b-200a-429 (chromosome 1) and 141-200c (chromosome 12). MiR-200 has been shown to be a master regulator of EMT, partially through the double-negative feedback loop with the transcriptional repressors ZEB1/2, maintaining the epithelial phenotype [11-15]. Previous studies have shown that loss of miR-200 is necessary and sufficient to drive EMT [16], yet the detailed mechanism on how the mesenchymal phenotype is maintained are not fully understood.

Recent studies have been focused on the importance of the ECM in mediating tumor cell activation, indicating that metastasis is driven by a combination of cell-intrinsic and cell-extrinsic changes. The miR-200/ZEB1 axis is known to regulate both, cell-intrinsic and cell-extrinsic changes, by modulating EMT markers and specific ECM components. Over the past years studies have shown that the ECM undergoes dramatic changes during tumor progression, affecting the tension in the surrounding microenvironment (e.g. through collagen fibers) as well as differential expression patterns of microRNAs and integrins, which further alter downstream signaling pathways [7, 17, 18]. Proteomic profiling of cell lines derived from our murine model showed differential expression of cell adhesion and ECM proteins in metastatic vs. non-metastatic cell lines [19].

Tumor cell-ECM interactions through integrins

The interaction of cells with the ECM is mainly mediated through integrins, heterodimeric receptors leading to the activation of downstream intracellular signaling pathways. There are 18 α and 8 β subunits whose pairs are unique to their

ligands. Structurally they are transmembrane glycoproteins with a large N-terminal extracellular domain, a single transmembrane domain and a short non-catalytic C-terminal intracellular tail. Many of the integrin subunits have been implicated to play an important role in cancer progression due to their role in migration and invasion in which they mediate the adhesion to the ECM and as result are able to regulate various intracellular signaling pathways. It is known that Integrins re-localize to adhesive structures causing alterations in their binding ability to the ECM. Once they bind to the ECM, cluster formation of the integrins is initiated, allowing for the recruitment of adaptor molecules, connecting the integrins with the actin cytoskeleton, kinases and other transmembrane growth-factor receptors. Integrins function through a bi-directional signaling: outside-in and inside-out. For the inside-out signaling, intracellular ligands (e.g. talins) cause the separation of the cytoplasmic tails which in turn promotes the binding of ECM ligands to the extracellular domain. The outside-in signaling is initiated by the binding of ECM ligands to the N-terminus, causing the separation of the cytoplasmic domains which allows for the interaction with adaptor molecules. It has been shown that increased integrin activation is necessary for cancer cell migration and metastases, even suggesting that cancer cells might use specific integrin-ligand combinations at distant sites to allow for colonization and to receive mitogenic signals. Integrin signaling, especially through β1, involves the activation of the focal adhesion kinase (FAK), leading to further downstream recruitment of adaptor molecules such as paxillin and p130cas [20, 21]. Blocking antibodies and a non-RGD (Arginyl-glycyl-aspartic acid) based peptide inhibitor have been used to inhibit Integrin β1 which

suppressed *in vitro* and *in vivo* growth of human breast cancer and the monoclonal antibody volociximab against α5β1 has shown good efficacy and tolerance in Phase I studies. Furthermore, the blocking antibody has been shown to increase apoptosis in 3D breast cancer models and sensitized cancer cells to irradiation in breast cancer xenografts [20, 22, 23].

Focal adhesions and FAK/Src signaling

Focal adhesions are considered clusters of transmembrane receptors of integrin and cytoplasmic proteins such as FAK and other adaptor molecules involved in downstream signaling [24]. FAK is a signaling kinase and adaptor scaffold protein with an auto-phosphorylation site at tyrosine 397 [25]. Upon FAK activation, its substrate Src is recruited, leading to further phosphorylation of the tyrosine residues 576/577, 861 and 925. Multiple studies have shown that activation of FAK promotes cell survival and motility. Furthermore, many cancers have increased FAK protein expression, which can lead to the formation of invasive structures such as podosomes and invadopodia, necessary for metastases [20, 25]. It has been shown that FAK is phosphorylated and re-localized to sites of focal adhesions in stiffer matrices, which are found upon the ECM remodeling occurring during tumor progression [8, 18]. Furthermore, FAK inhibition using siRNA has been demonstrated to increase cell-cell adhesion, an epithelial characteristic, through E-cadherin modulation and to reduce cell invasion [21].

FAK and many of the adaptor molecules involved in focal adhesion signaling are known Src substrates. Src is one of the 11 Src-family kinase members, which contains an auto-phosphorylation site in the activation loop. In addition to the

positive regulatory site at residue Y416 (auto-phosphorylation site) it also has a negative regulatory site at residue Y527. The tyrosine kinase Src is an oncogene that is overexpressed in many cancer types and known to be involved in multiple cellular processes, such as proliferation, cell morphology, migration, invasion and adhesion. It is negatively regulated by the C-terminal Src kinase (CSK) which phosphorylates Src at residue Y527 to inactivate Src [26]. Furthermore, Src is regulated by protein tyrosine phosphatases which de-phosphorylate Src at its negative regulatory site. The tyrosine kinase acts as signal transducer from cell surface receptors (e.g. integrins) through phosphorylation of tyrosine residues on substrates such as FAK, Cas and paxillin. Src inhibition has been shown to decrease migration *in vitro*, tumor growth and invasion *in vivo* in NSCLC using murine xenograft models [27, 28]. Furthermore, inhibition of Src using the ATP binding competitive inhibitor Dasatinib decreased the development of liver metastases in a murine model of pancreatic carcinoma and caused a decrease in cell adhesion, migration and invasion in colon cancer cell lines. In thyroid cancer cell lines, Dasatinib was shown to have a cytostatic activity both *in vitro* and *in vivo* causing cell cycle arrest and an increase in senescence [29]. Yet, Dasatinib has only been used on patients with advanced disease and therefore not been proven successful in clinical trials. In addition to Dasatinib, the more specific Src inhibitor Saracatinib (AZD0530) has been used in multiple studies resulting in a growth inhibition in several cancer cell lines and reduced migration and invasion [30]. Combination treatment of Saracatinib with an EGFR/HER2 drug in breast cancer

has shown to cause cell cycle arrest and as result suppressed the formation of brain metastases which are normally promoted by Src [31].

The formation of the FAK/Src complex at sites of focal adhesions is necessary in mediating cell-matrix contacts and cytoskeletal reorganization, mostly through regulating the phosphorylation status of the cytoskeletal protein cortactin, which is involved in cell adhesion, migration and invasion [25, 32]. The focal adhesion complex formation is facilitated by adaptor molecules such as CRKL, linking the cell-matrix interactions to intracellular signaling activation [33].

CRKL

CRKL, an integrin adaptor molecule, belongs to the family of CRK proteins, known to control transcription and the cytoskeleton through downstream signaling cascades. They are activated through extracellular and intracellular stimuli, such as growth factors, cytokines and the tyrosine kinase Bcr-Abl, respectively. CRKL has been implicated to play a role in proliferation, adhesion, survival, migration and invasion [34, 35]. It has been found to be overexpressed in many cancer types, including lung, breast, skin, ovarian and colon cancer, primarily leading to enhanced adhesion to fibronectin, an ECM protein [33, 36-38]. Furthermore, the phosphorylation status of CRKL is used as a prognostic factor for CML survival [39]. It is known to directly interact with paxillin and p130Cas and translocates to focal adhesions upon Src activation [40].

This study is focused on understanding how the miR-200/ZEB1 axis controls the matrix-dependent tumor cell activation by modulating cell-cell and cell-matrix interactions and cytoskeletal changes, necessary to drive the invasive phenotype.

Chapter 2

Materials and Methods

Animal studies.

All animal experiments were approved by the *institutional animal care and use committee* (IACUC) at the University of Texas M.D. Anderson Cancer Center. Wild type male and female mice from the 129/sv strain with a minimum age of 2 months were used for the mice experiments. 0.5 -1 x 10^6 cells were subcutaneously injected in the flank in a volume of 100 µl in serum free RPMI. The animals received intraperitoneal injections 5 days a week with dasatinib (purchased from Selleckchem) at a dose of 10 mg/kg or 20 mg/kg in a volume of 50 µl or the vehicle DMSO. The animals were monitored for tumor burden and sacrificed once the tumor size exceeded 15 mm or euthanized due to tumor ulcerations. Mice were examined for metastasis and tissues for the subcutaneous tumor, lungs and any organs with visible metastasis were collected. The results are represented as mean ± standard deviation and student's *t*-test was performed for statistical significance.

Cell culture.

Cell lines derived from the mutant Kras and p53 lung adenocarcinoma mouse model (previously published [16]) and human lung cancer cells H157 were cultured in RPMI1640 with 10 % fetal bovine serum (FBS) (Table 1). HEK 293T cells were cultured in DMEM with 10 % fetal bovine serum (FBS).

Cell line	Species
393LN	murine
412P	murine
393P	murine
307P	murine
531P1	murine
531LN2	murine
531LN3	murine

344LN	murine
531LN1	murine
344P	murine
344SQ	murine
344SQ_200	murine
393P_vec	murine
393P_ZEB1	murine
393_ZEB1_vec	murine
393P_ZEB1_200	murine
H157	human
H157 pTRIPZ	human
H157 200ab	human

Table 1. Cell lines used in the study

Inhibitors and blocking antibodies.

The inhibitors dasatinib, AZD0530 and imatinib were a kind gift from Dr. Faye Johnson (MD Anderson). TGF-β was purchased from Cell Signaling (#8915LF). FAK inhibitor 14 (Y15) was purchased from Santa Cruz (sc-203950). All blocking antibodies and Ig controls were purchased from BD Biosciences and used at a final concentration of 8 μg/ml: Itgβ1 (BD 555002), Itgβ3 (BD 553343), IgM (BD 553957), IgG (553950).

Generation of pLenti6.3 Src dominant active (DA) and dominant negative (DN) constructs.

Src DA Y527F and Src DN K295R plasmids were purchased from Addgene (Plasmid 17675 and 17678). Following the Gateway® Technology cloning manual PCR primers were designed adding attB sites to each of the Src DNA sequences (Src attB F: GGGGACAACTTTGTACAAAAAAGTTGGCATGGGGAGCAGCAAGA GC, Src attB R: GGGGACAACTTTGTACAAGAAAGTTGGGCTATAGGTTCTCTCC

AGG). The obtained PCR products were further cloned into a pDONR221 vector using a BP reaction (Invitrogen 56481) and the resulting plasmids cloned into the Destination vector pLenti6.3 EF (kindly provided by Dr. Kenneth Scott, Baylor College of Medicine) using a LR reaction (Invitrogen 56484). The final plasmids were confirmed using Sanger sequencing and used for lentiviral infection.

Lentivirus transfection.

Lentiviral-based Itgβ1 shRNA were purchased from Thermo Scientific (mouse: TRCN0000066643, TRCN0000066644, TRCN0000066645, TRCN0000066646, TRCN0000066647 (also targets human Itgβ1), human: TRCN0000029645, TRCN0000029648). Lentiviral-based CRKL shRNA were purchased from Thermo Scientific (mouse: TRCN0000097199, TRCN0000097200, TRCN0000097202, TRCN0000097203). Murine Csk cDNA was purchased from Origene (MC203625) and cloned into the pTRIPZ-GFP vector. 293T cells were seeded one day prior to transfection. 2 μg DNA construct, 1.5 μg psPAX2 (gag-Pro-Pol, for packaging) and 0.5 μg pMD2.G (envelope plasmid) were mixed and added to Opti-MEM® (GIBCO). PLUS™ reagent (Invitrogen) was added to the mixture and incubated for 5 minutes at room temperature. After addition of Lipofectamine® LTX (Invitrogen), the mixture was incubated for 30 minutes at room temperature and added to the cells. 8-12 hours post-transfection, the transfection mixture was replaced with fresh DMEM. Virus was collected 3 times every 12 hours after a 24 hour recovery period and stored on ice at 4 °C. The virus was filtered using a 0.45 μm syringe filter and polybrene (8 μg/ml, Millipore) was added for efficient infection and incubated for 10 minutes at room temperature. The target cells (344SQ,

393P_ZEB1 and H157) were infected 2 times with the virus (with an 8 hour time period in between infections). The virus was replaced with fresh RPMI 12 hours past the 2nd transfection and after a 24 hour recovery period antibiotic selection was started.

siRNA transfection.

The human CRKL siRNA SMARTpool was purchased from Dharmacon (L-012023-00-0005) and used at a final concentration of 25 nM. One day before transfection, cells were plated in 6 well plates. The siRNA and DharmaFECT I (Dharmacon) were separately diluted in serum-free RPMI and incubated for 5 minutes at room temperature. The diluted siRNA was added to the DharmaFECT mix and incubated for 20 minutes at room temperature before adding it to the cells. RNA and lysates were collected 48 hours post transfection.

Migration and Invasion Assay.

Cells were seeded at a density of 5 x 10^4 per well in serum-free media in a 24-well Transwell or Matrigel plate (BD Biosciences, pore size 8 μm). RPMI with 10 % FBS was placed in the lower chamber as a chemoattractant and cells were allowed to migrate for 6 hours (H157 cells) or 16 hours (murine cells) at 37 °C at 5 % CO_2. The migrated/invaded cells were stained with 0.1 % crystal violet and non-migrated/invaded cells in the upper chamber removed using a cotton swab. Five microscopic fields at a 4x magnification were captured from each well and migrated/invaded cells counted. The results are represented as mean ± standard deviation and student's *t*-test was performed for statistical significance. The graphs in each figure represent one experiment. Each assay was performed in triplicates.

Cell Adhesion Assay.

Wells of a 24 well plate were coated with a thin layer of either Fibronectin (10 µg/ml, Sigma F1141), Matrigel, Matrigel/Collagen type I (final concentration 1.5 mg/ml) or Collagen type I (final concentration 1.5 mg/ml, Corning). Cells were pre-treated with Y15 (5 µM) for 24 hours before 50,000 cells/well were plated. After the incubation time, each well was washed twice with PBS to remove unattached cells, fixed for 10 minutes at room temperature with 10 % formalin, washed with PBS and stained using 0.1 % Crystal Violet/PBS. Images are representatives of the triplicates performed for each condition. For the washout experiment, pre-treated cells were washed and added to the wells without Y15. Quantification of cell adhesion was measured by the absorbance at 595 nm after dissolving the crystal violet stained cells in 10 % acetic acid for 20 min.

Quantitative Real-Time PCR.

RNA was isolated using TRIzol® Reagent (Invitrogen) according to the manufacturer's protocol and reverse transcribed into cDNA using qScript™ Reagent (Quanta Biosciences) or iScript™ (Bio-Rad). mRNA levels were measured using SYBR® Green-based detection (Applied Biosystems) on an ABI 7500 Fast Real-Time PCR System (Applied Biosystems). The primers were designed using the NIH primer design tool. For each gene a dissociation curve was generated and the results of each sample normalized to the ribosomal protein L32, which serves as internal control. All measurements were performed in triplicate and expressed as mean ± standard deviation. Student's *t*-test was performed for statistical significance. Analysis of the microRNA levels was performed following the TaqMan

microRNA protocol (Applied Biosystems) and results were normalized to the control miR-16. All TaqMan probes were purchased from Life Technologies (miR-200a Assay ID: 000502, miR-200b Assay ID: 001800, miR-200c Assay ID: 000505, miR-141 Assay ID: 000463, miR-429 Assay ID: 001077, miR-16 Assay ID: 000391). Primer sequences are listed in (Table 2).

qPCR primer 5' to 3'	
ms L32: F	GGAGAAGGTTCAAGGGCCAG
ms L32: R	TGCTCCCATAACCGATGTTG
ms Zeb1: F	ATGCTCTGAACGCGCAGC
ms Zeb1: R	AATCGGCGATCTTTGAGAGCT
ms CDH1: F	CCATCTCAAGCTCGCGGATA
ms CDH1: R	TCCAACGTGGTCACCTGGT
ms CDH2: F	TCCAGAGGGATCAAAGCCTGGGAC
ms CDH2: R	CCGCATCAATGGCAGTGACCGT
ms Vim: F	TCCAAGCCTGACCTCACTGC
ms Vim: R	TTCATACTGCTGGCGCACAT
ms Crb3: F	CGGACCCTTTCACAAATAGCA
ms Crb3: R	CGTTGGACTCATCACCTGGG
ms Itgb1: F	CTACTTCTGCACGATGTGATGAT
ms Itgb1: R	TTGGCTGGCAACCCTTCTTT
ms Itgb2: F	CAGGAATGCACCAAGTACAAAGT
ms Itgb2: R	CCTGGTCCAGTGAAGTTCAGC
ms Itgb3: F	CCACACGAGGCGTGAACTC
ms Itgb3: R	CTTCAGGTTACATCGGGGTGA
ms Itgb4: F	AGAGCTGTACCGAGTGCATC
ms Itgb4: R	TGGTGTCGATCTGGGTGTTCT
ms Itgb6: F	GAAAACCCTGTCTCCCGCATA
ms Itgb6: R	CGCTGAGAGGCTTATTTTGAAGG
ms Itgb7: F	ACCTGAGCTACTCAATGAAGGA
ms Itgb7: R	CACCGTTTTGTCCACGAAGG
ms CSK: F	AAGGTGGAGCACTACCGCATCA
ms CSK: R	AGAGTCCATCGGCATCTGTGGT
ms Src: F	GAGTCACGGACAGAGACTGA
ms Src: R	GACATCCACCTTCCTCGTGT
ms CRK: F	CTAATGCCTACGACAAGACAGCC
ms CRK: R	TGGGAAGTGACCTCGTTTGCCA
ms CRKL: F	CCTGGACACTACCACCTTAATCG

ms CRKL: R	TCTTCTGCTGTAGGTAAGTTGGG
ms PINCH1: F	GGGTTTGTCAAGAATGCTGGCAG
ms PINCH1: R	GCACAGTTGAAGTGGTCTGGATG
ms NEDD9: F	TCTAAGCAAGGACCAGCCACCA
ms NEDD9: R	CTCCTTCTGCTGTCGCTCAAAC
ms ILK: F	GTGCTGAAGGTTCGTGACTGGA
ms ILK: R	TCCAGTGTGTGATGAGGGTTGG
hs L32: F	CCTTGTGAAGCCCAAGATCG
hs L32: R	TGCCGGATGAACTTCTTGGT
hs Zeb1: F	GGCATACACCTACTCAACTACGG
hs Zeb1: R	TGGGCGGTGTAGAATCAGAGTC
hs Itgb1: F	GGATTCTCCAGAAGGTGGTTTCG
hs Itgb1: R	TGCCACCAAGTTTCCCATCTCC
hs_CRKL Ori: F	ATCCACTACCTGGACACCACCA
hs_CRKL Ori: R	CCAGGTTATCTTCTGCTGTAGGC

Table 2. Primer sequences used for qPCR analysis

Western Blot Analysis.

Cell lysates were prepared according to the RIPA buffer protocol (CS 9806). Samples were separated using sodium dodecyl sulfate polyacrylamide gel electrophoresis and transferred onto Nitrocellulose or polyvinylidene difluoride (PVDF, for p-CRKL antibody only) membranes. The membranes were blocked using 5 % nonfat dry milk and incubated in primary antibody overnight at 4 °C (see Table 3 for antibody list).

Protein	**Company**	**Catalog Number**
Cortactin	MilliPore	05-180
Crkl	MilliPore	05-414
Crkl pY207	Cell Signaling	3181
Csk	BD Pharmingen	610080
Cttn pY421	Invitrogen	44854
Cttn pY421	Abcam	47768
E-Cadherin	BD Pharmingen	610182

FAK	Invitrogen	AHO0502
FAK pY397	Invitrogen	44624G
FAK pY576/577	Cell Signaling	3281
FAK pY861	Invitrogen	44-626G
FAK pY925	Cell Signaling	3284
GFP	Santa Cruz	9996
Integrin β1	Cell Signaling	4706
N-cadherin	BD Pharmingen	610921
p130Cas	Upstate	06-500
p130Cas pY410	Cell Signaling	4011
Paxillin	BD Pharmingen	610620
Paxillin	Abcam	2264
Paxillin pY118	Abcam	4833
Src	Cell Signaling	2108s
Src pY416	Cell Signaling	2101L
Src pY418	MilliPore	569373
Src pY527	Cell Signaling	2105
Vimentin	Cell Signaling	3932S
Zeb1	Santa Cruz	25388

Table 3. List of antibodies used for Western Blot analysis

3D culture.

Cells were grown in 8-well chamber slides coated with Matrigel (BD 356231) or Matrigel/Collagen (BD 354249, at the indicated Collagen concentration), as previously described. [16] The media (RPMI with 10 % FBS and 2 % Matrigel) was replaced every 2-3 days and the morphology of the cells monitored using a light microscope. Size of the structures and invasion were scored at the end of the experiment, with structures being counted invasion-positive if ≥ 1 protrusions were present. Immunofluorescent staining of the 3D cultures was performed as previously described [16]. Protein isolation from 3D assays was performed using PBS-EDTA as previously described [41]. In brief, each well was washed with ice-cold PBS before adding PBS-EDTA. The Matrigel or Matrigel/Collagen layer was detached from the glass slide, transferred into a falcon tube and briefly vortex to ensure disruption of

the layer. The mixture was left on ice for 25 minutes until a pellet formed and centrifuged at 115 g for 5 minutes. The pellet was washed twice with PBS-EDTA and spun at 4,000 rpm for 2 minutes before the cells were lysed with RIPA buffer for 30 minutes on ice. The lysate was cleared by centrifugation and protein estimation performed. For dissolving the Matrigel/Collagen layer, a Collagenase treatment was performed after the initial wash. Each well was incubated with Collagenase Type I (1,000 U/ml, Calbiochem #234153) for 30 minutes at 37 °C.

Immunohistochemistry.

All tissues were formalin fixed and paraffin embedded. The paraffin embedded tissue sections were deparaffinized in xylene twice for 5 minutes at room temperature followed by hydration of the samples in graded ethanol (twice 100 %, twice 95 %, 80 %) for 5 minutes each at room temperature. Antigen retrieval was performed in citrate buffer (DAKO #S1699) for 25 minutes at 95 °C and allowed to cool for 20 minutes. Endogenous peroxidase activity was blocked by incubating the slides in 3 % H_2O_2 diluted in methanol for 5 minutes. Non-specific protein-protein interactions were blocked using serum-free protein block (DAKO #X0909) for a minimum of 1 hour at room temperature. The primary antibody p-Src Y^{418} (MP569373) was added to the slides at a dilution of 1:50 overnight at 4 °C. For the negative controls, goat serum was added. After washing with TBST, slides were treated with a secondary biotinylated antibody (1:300, DAKO #0353) for 30 minutes at room temperature followed by incubation with peroxidase-conjugated streptavidin (1:100, DAKO #P0397) for 30 minutes. Visualization of the antibody staining was performed by adding Chromagen substrate diluted in DAB buffer (DAKO #K3468)

followed by a counterstain in Hematoxylin for 6 minutes and Scott's Bluing Reagent. Slides were dehydrated in graded ethanol for one minute each (80 %, 95 %, 100 %) followed by incubation in xylene twice for 10 minutes each.

Immunofluorescence.

Acid-washed 18 mm coverslips were coated with either 50 µg/ml poly-L-lysine or fibronectin (10 µg/ml) before 20,000 cells were plated and grown overnight. Cells were fixed with 4 % paraformaldehyde/PBS for 20 minutes at 37 °C and washed three times with PBS. Permeabilization was performed using 0.1 % Triton X-100 for 10 minutes at room temperature followed by three PBS washes. The coverslips were blocked for a minimum of 1 hour at room temperature with 5 % goat serum/PBS before the primary antibodies were added overnight at 4 °C (Cortactin Millipore 05-180, 1:1000; p-Src Y^{418}, Millipore 569373, 1:50; p-FAK Y^{861} Invitrogen 44626, 1:50; Paxillin BD610620, 1:100). After three washes with PBS, the coverslips were incubated with secondary antibodies labelled with Alexa Fluor® 488 or 546 (Life Technologies) for 2 hours at room temperature. Staining of F-actin was performed using Alexa Fluor® 546 Phalloidin (Life Technologies). After the secondary antibody incubation the coverslips were mounted onto microscope slides using a DAPI containing mounting solution for the nuclear stain.

Luciferase Reporter Assay.

The three prime untranslated regions (3'-UTRs) were amplified by PCR from genomic DNA and mutants generated using a QuikChange® II XL site-directed mutagenesis kit (Stratagene), which were further cloned into the hRL vector. One day before transfection, 3 x 10^4 cells were seeded in 24 well plates and co-

transfected with 50 ng pGL3 control vector and 500 ng hRL constructs. Pre-miRs were added at a final concentration of 30 nM (Ambion). After 48 hours Luciferase activity was measured following the protocol for the Dual-Luciferase® Reporter Assay (Promega).

Cytosol/Particulate Separation.

The separation of cytosol and particulate was performed using a cytosol/particulate rapid separation kit purchased from BioVision (#K267-50). The workflow is depicted in Fig. 1.

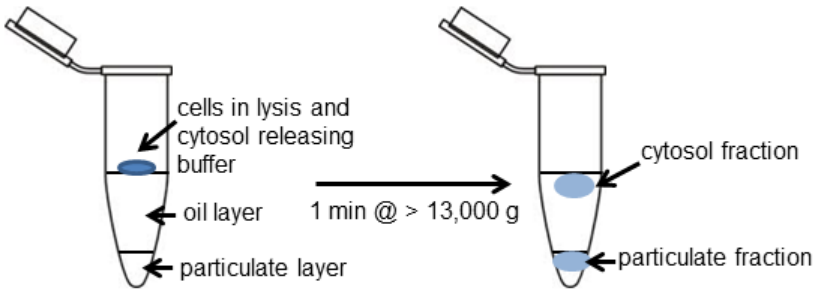

Fig. 1 Workflow of cytosol/particulate separation. Using this separation method the cytosol and particulate fractions do not come into contact therefore contaminations can be avoided.

Chapter 3

Results

Zeb1 expression induces a functional EMT in epithelial, non-invasive tumor cells.

Our previous work with metastasis-prone tumor cells from the KP murine model revealed that miR-200 repression is necessary in a subset of cells at the tumor periphery for EMT and metastasis [16, 42]. To test whether Zeb1 expression in tumorigenic, but non-metastatic cells was sufficient to induce a mesenchymal and invasive phenotype similar to that observed in the metastasis-competent cells, stable transfectants were generated with constitutive Zeb1 expression. Constitutive Zeb1 expression in the epithelial 393P cells from the KP model produced a dramatic morphologic change, with cells displaying a spindle-like, fibroblastic shape (Fig. 2A & B). This change was partially reversed by re-expression of miR-200, as seen in the lower panel of (Fig. 2A). F-actin staining demonstrated that the mesenchymal, invasive 344SQ and 393P_ZEB1 cells display cell protrusions, long actin stress fibers and enhanced cell matrix contact, which were lost upon miR-200 expression (Fig. 2B). The morphologic change observed with Zeb1 was concordant with an EMT, as shown by the mRNA and protein levels of epithelial and mesenchymal markers (Fig. 3A) and decreases in the miR-200 family (Fig. 3B). As a functional consequence, Transwell migration and invasion were enhanced in the previously non-invasive 393P cells, and suppressed upon miR-200 re-expression (Fig. 3C). Similar results were obtained with a doxycycline-inducible system to express miR-200a and/or b in the human H157 lung cancer cell line, producing an MET with morphologic reorganization into tight epithelial clusters (Fig. 4A), suppression of mesenchymal and re-expression of epithelial protein markers (Fig. 4B), with the

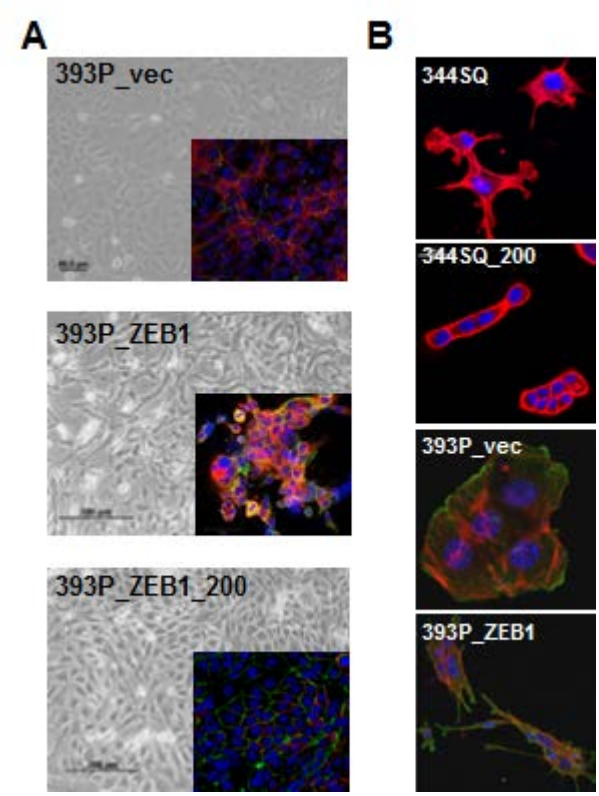

Fig. 2 Zeb1 expression induces EMT. (A) Zeb1 expression causes a morphology change (middle panel) and is reversed upon re-expression of miR-200 (lower panel). Cells were stained with Integrin α6 (red), ZO-1 (green) and DAPI. (B) Cells grown on agarose and stained with phalloidin (red), DAPI and cortactin (green, lower panels).

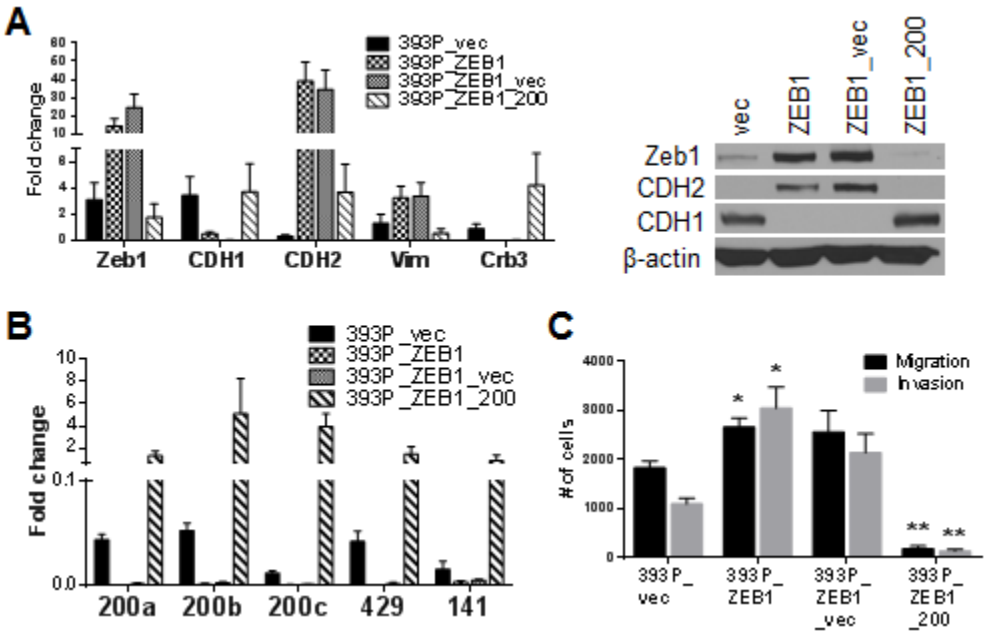

Fig. 3 Zeb1 expression induces EMT/miR-200 repression in previously non-invasive cells. (A) Quantitative RT-PCR (left) and Western Blot (right) analysis of EMT markers in the indicated cell lines. (B) Taqman RT-PCR for the miR-200 family members in the indicated cell lines. (C) In vitro migration and invasion assay for the 393P cell line panel. * $p < 0.004$, ** $p < 0.001$

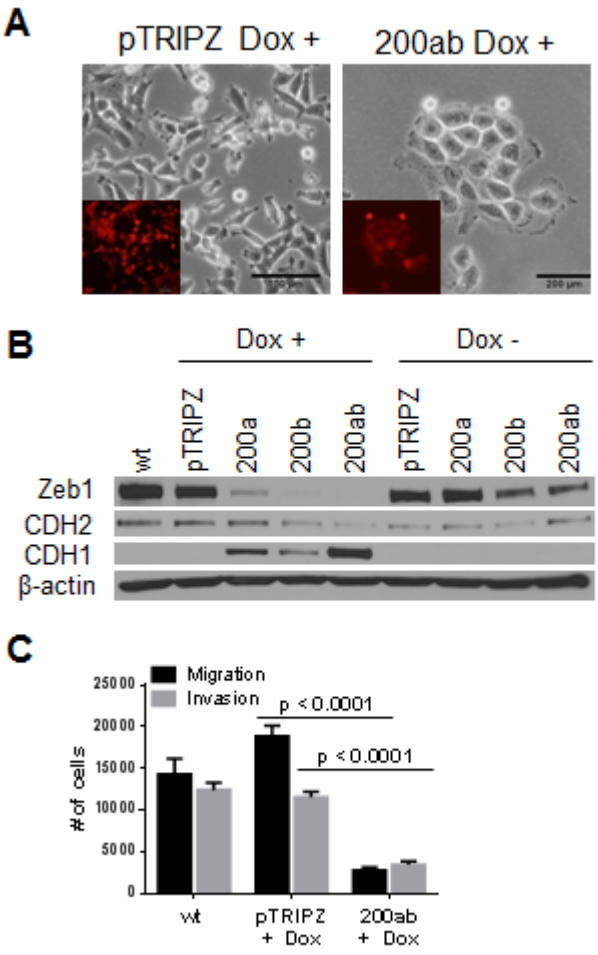

Fig. 4 Loss of miR-200 in human H157 cells causes an MET. (A) Induction of miR-200a and b in H157 causes a morphology change. (B) Western Blot analysis of EMT markers in H157 +/- miR-200a and/or b. (C) In vitro migration and invasion assay for the inducible H157 cells.

most pronounced effect seen upon combined miR-200a and b expression. The induction of MET in H157 cells upon miR-200 induction significantly suppressed the migratory and invasive ability of the cells in Transwell assays (Fig. 4C).

miR-200 repression alters cell-cell and cell-matrix interactions.

We utilized a well-established 3D culture assay to study the importance of the ECM in regulating tumor cell behavior in coordination with Zeb1/miR-200 expression changes [41]. To model the extracellular matrix composition found in tumors, cells were grown on a Matrigel matrix or a mixture of different Matrigel/collagen type I concentrations and then stained for markers to reveal the differential 3D organization. Control cells grew as rounded, non-invasive colonies in all conditions, but upon Zeb1 expression displayed a progressively invasive response upon growth in collagen type I, dependent upon the collagen concentration (Fig. 5A, middle row, and Fig. 5B). At the highest collagen concentration, ~70% of the colonies were invasive. Upon re-expression of miR-200 the cells displayed a more organized epithelial acinar structure in Matrigel culture, with pronounced cortical actin staining, and suppression of the collagen-induced invasion (Fig. 5A, bottom row). These results suggest that miR-200 repression enhances the response of the cells to external stimuli from the ECM, producing a highly invasive phenotype.

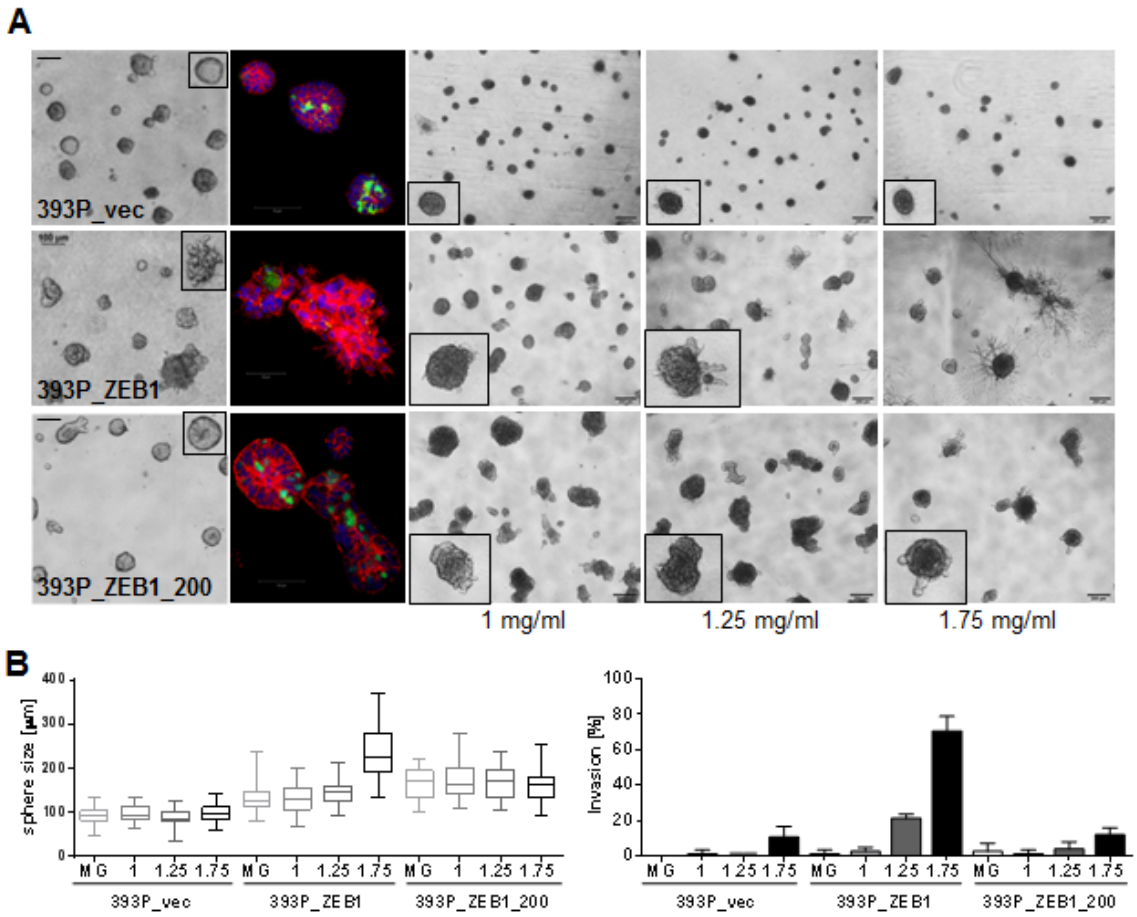

Fig. 5 miR-200 repression primes cells to external stimuli and causes alterations in cell-cell & cell-matrix interactions. (A) Morphology of spheres grown in a Matrigel matrix (left two columns) and stained with Integrin α6 (red), ZO-1 (green) and DAPI; or grown in a mixture of Matrigel and collagen I at the indicated concentrations. (B) Quantification of the spheres grown in Matrigel (MG) and Matrigel/collagen I at day 7. For each condition 30 structures were measured in size and 75 structures scored for invasiveness.

Integrin β1 is necessary for the invasion of murine mesenchymal cell lines.

Integrins are important sensors of the cellular environment, transducing changes in the surrounding ECM to drive intracellular signaling. Based upon the altered responsiveness of tumor cells to collagen I in the matrix upon loss of miR-200, we screened for changes in the expression or functionality of integrin subunits induced by EMT. Screening of multiple integrin β subunits revealed that Itgβ1 is highly expressed in the mesenchymal 393P_ZEB1 cells. Additionally, Itgβ1 was up-regulated in the 2D vs. 3D cultures of 344SQ, paralleling the normal changes in miR-200 expression upon 3D growth (Fig. 6A). Western Blot analysis of the murine cell panel showed expression of Itgβ1 in epithelial and mesenchymal cell lines, with only slightly higher expression in the mesenchymal cells (Fig. 7A). We next investigated the functional effect of an Itgβ1-blocking antibody on tumor cell invasion in 3D cultures. The antibody significantly decreased the invasive ability of 393P_ZEB1 cells when grown in Matrigel/collagen I (Fig. 7B), as compared to an Itgβ3-blocking antibody that produced no effect (Fig. 6B). In addition, combined treatment of Itgβ1 and Itgβ3-blocking antibodies showed a dominant effect of Itgβ1 over Itgβ3, as addition of α-Itgβ1 at day 4 when cells were beginning to form invasive structures, still blocked the invasive phenotype. To further confirm the importance of Itgβ1 in mediating invasion, we used an shRNA-based knockdown approach to deplete highly invasive 393P_ZEB1 cells of Itgβ1, as confirmed by mRNA and protein levels (Fig. 8A). Knockdown of Itgβ1 caused a significant reduction in Transwell invasion for all of the tested shRNAs, blunted migration for three of the four tested shRNAs (Fig. 8B), and produced a shift to a more epithelial phenotype (Fig. 8C). Strikingly,

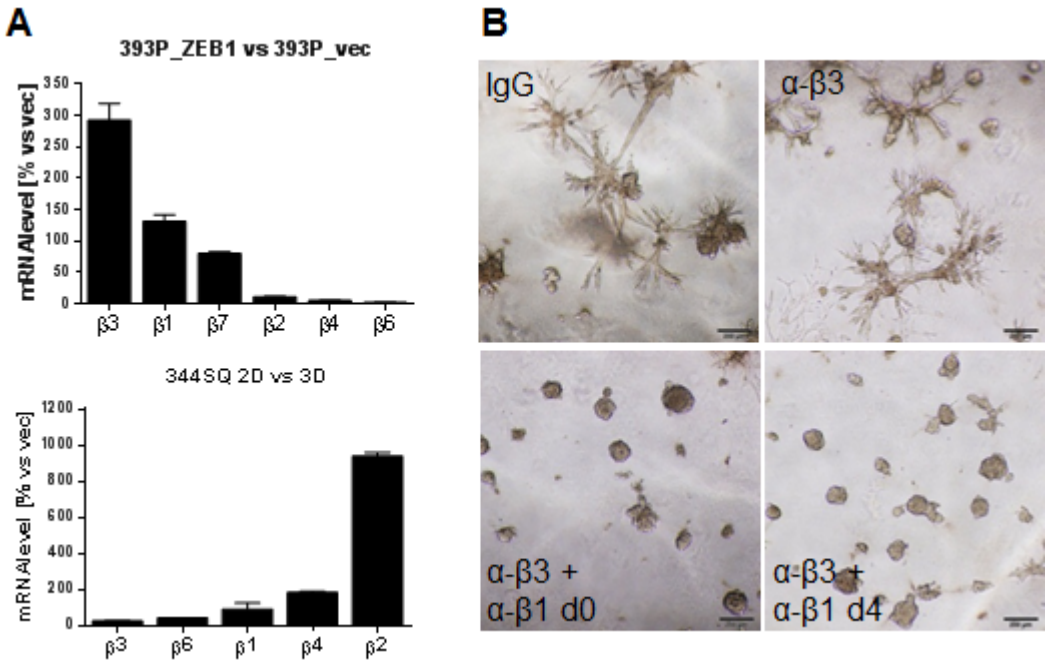

Fig. 6 Integrin β1 is required for mesenchymal cell invasion. (A) Quantitative RT-PCR analysis of Integrin β subunits in 393P_ZEB1 vs vec cells (top panel) and in 344SQ grown in 2D vs 3D Matrigel (lower panel) (B) 393P_ZEB1 cells grown in 1.75 mg/ml Matrigel/collagen I and treated with an Integrin β3-blocking antibody alone, in combination with an Integrin β1-blocking antibody (added at the days indicated) or IgG control for 7 days.

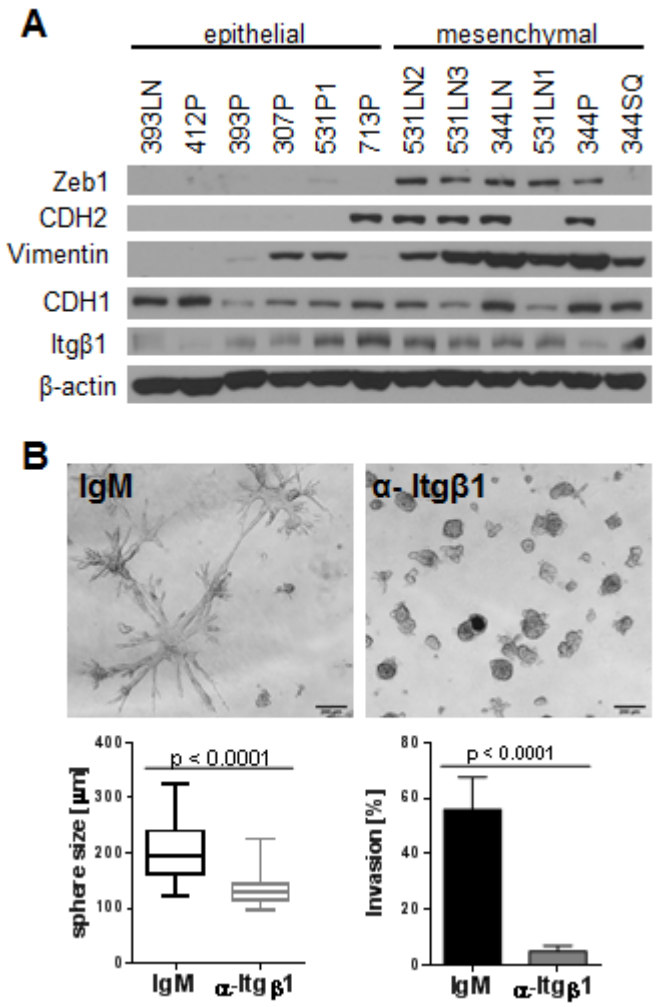

Fig. 7 Integrin β1 inhibition blocks 3D invasion in murine mesenchymal cell lines. (A) Integrin β1 expression in the murine cell line panel. (B) 393P_ZEB1 cells grown in 1.75 mg/ml Matrigel/collagen I and treated with an ITGβ1-blocking antibody or IgM control for 7 days.

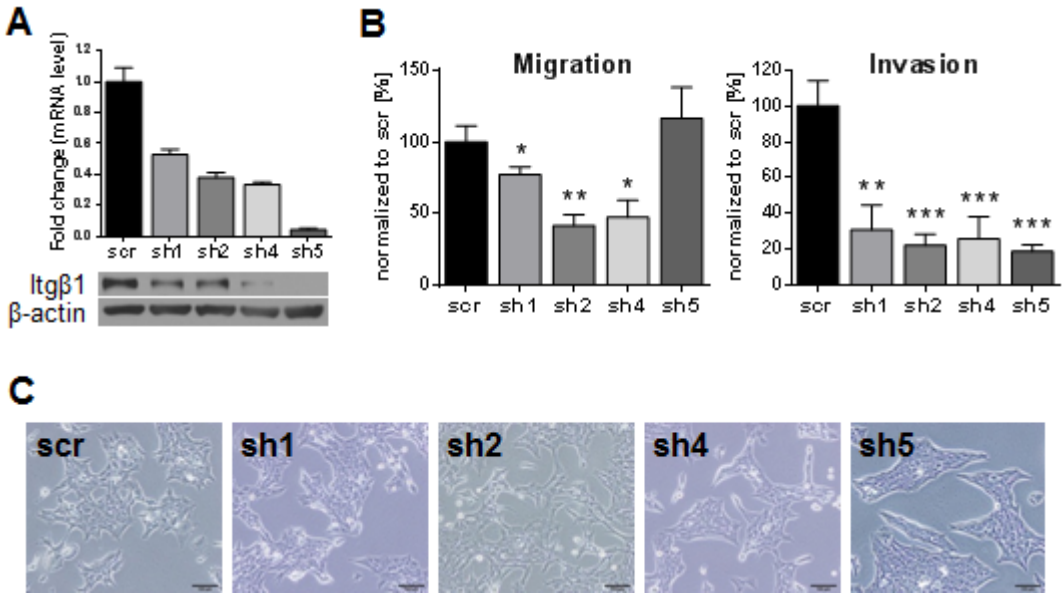

Fig. 8 Integrin β1 knockdown blocks 2D invasion in murine mesenchymal cell lines. (A) Quantitative RT-PCR and Western Blot analysis of 393P_ZEB1 cells after ITGβ1-shRNA knockdown. (B) In vitro migration and invasion assay for the Itgβ1 shRNA cells. * $p < 0.02$, ** $p < 0.002$, *** $p \leq 0.001$ (C) Morphology of 393P_ZEB1 cells after Itgβ1 knockdown.

the Itgβ1 shRNA inhibited 3D invasion in Matrigel/collagen I cultures of 393P_ZEB1 cells to a similar degree as the Itgβ1-blocking antibody (Fig. 9A). We further depleted the highly metastatic 344SQ cells of Itgβ1, as confirmed by mRNA and protein levels (Fig. 10A). All of the tested shRNAs showed a significant reduction in Transwell invasion without any effect on the migration (Fig. 10B), as well as a morphology change to a more epithelial phenotype in shRNA 5 (Fig. 10C). In order to see if Itgβ1 knockdown can blunt TGFβ-induced EMT, the shRNA cells were grown in Matrigel in 3D and treated with TGFβ, which normally causes a hyper-proliferative and highly invasive phenotype. Itgβ1 knockdown caused a significant reduction in the responsiveness to TGFβ, as quantified by sphere size and invasion (Fig. 10D). In addition, knockdown of Itgβ1 significantly decreased the number of lung metastases *in vivo* (Fig. 11). Moreover, widespread metastases were found in the liver, kidneys, intestines, heart, rib cage and diaphragm of the control mice but none were observed in the mice who received tumor cells with Itgβ1 knockdown (Fig. 11).

Integrin β1-collagen I contact is necessary for H157 cell growth and invasion.

To confirm the effect of the Itgβ1-blocking antibody with human cells, we treated the mesenchymal H157 cells with α-Itgβ1 either from day 0 or day 7, when the cells were starting to form invasive structures. In both treatment groups, 3D invasion was significantly inhibited (Fig. 12A), confirming the observations with the murine cells . shRNA-based knockdown of Itgβ1 produced a partial MET with

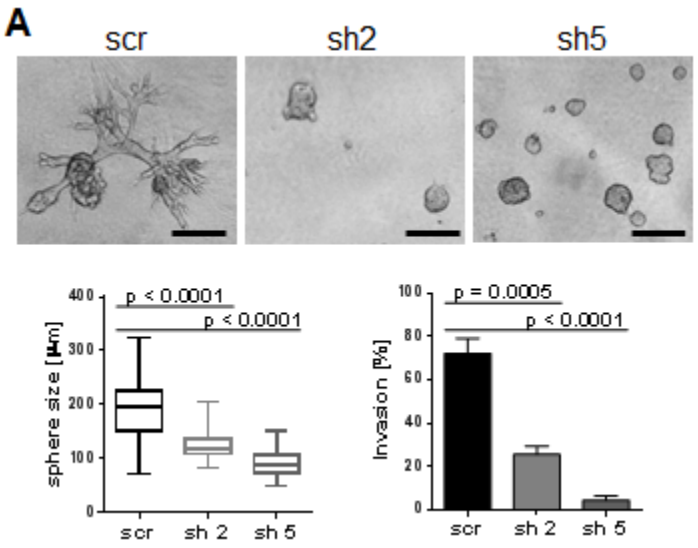

Fig. 9 Integrin β1 shRNA knockdown blocks 3D invasion in murine mesenchymal cell lines. (A) 393P_ZEB1 Itgβ1 shRNA cells grown in 1.75 mg/ml Matrigel/collagen I at day 6. For each condition 30 structures were measured in size and 90 structures scored for invasiveness. Scale bar represents 200 µm.

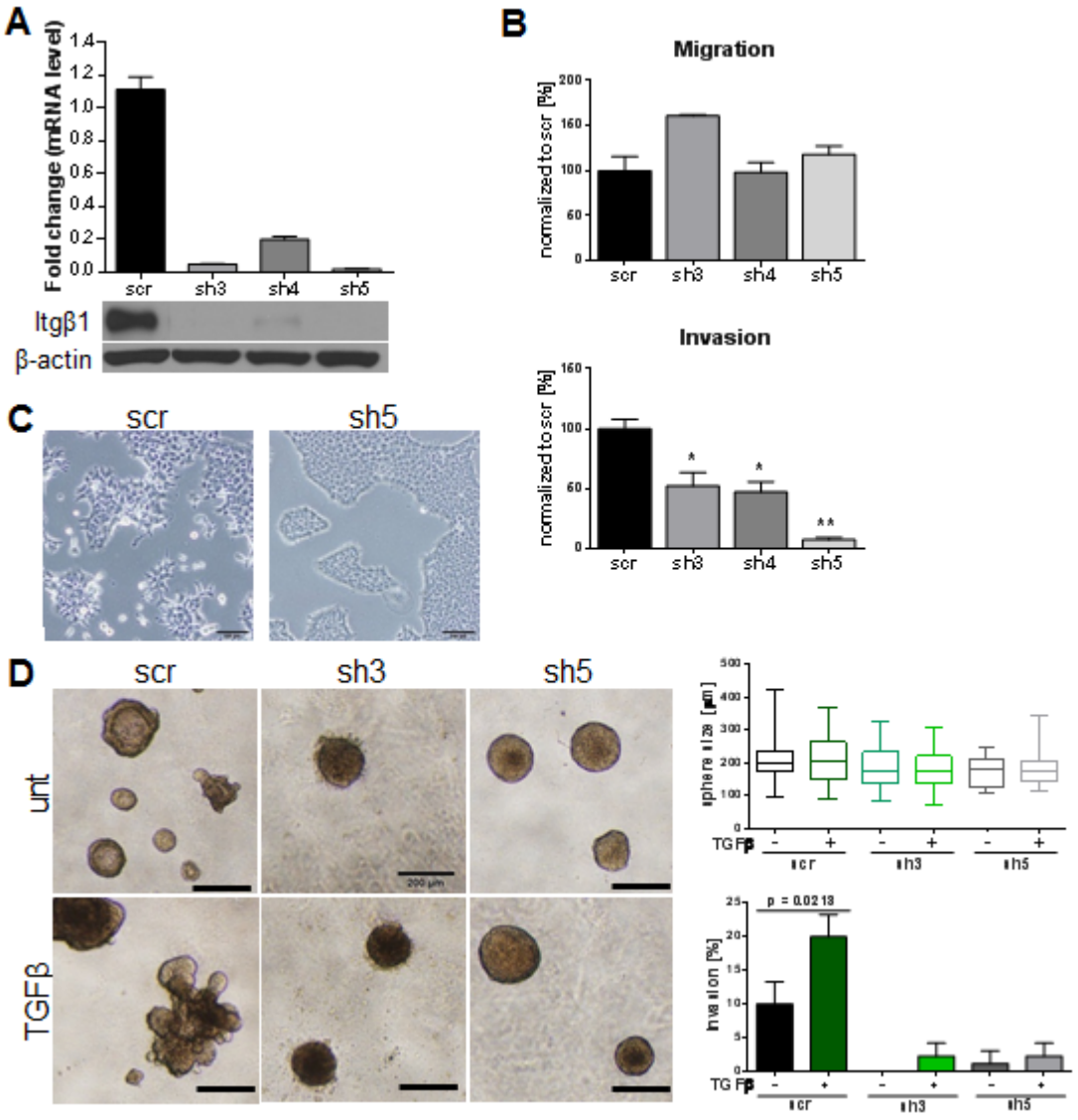

Fig. 10 Integrin β1 knockdown blocks 2D invasion and 3D responsiveness to TGFβ in murine mesenchymal cell lines. (A) Quantitative RT-PCR and Western Blot analysis of 344SQ cells after ITGβ1-shRNA knockdown. (B) In vitro migration and invasion assay for the Itgβ1 shRNA cells. * $p < 0.015$, ** $p = 0.0002$ (C) Morphology of 344SQ cells after Itgβ1 knockdown. (D) 344SQ Itgβ1 shRNA cells grown in Matrigel at day 11. TGFβ treatment (1 ng/ml) was started at day 6. For each condition 30 structures were measured in size and 90 structures scored for invasiveness. Scale bar represents 200 µm.

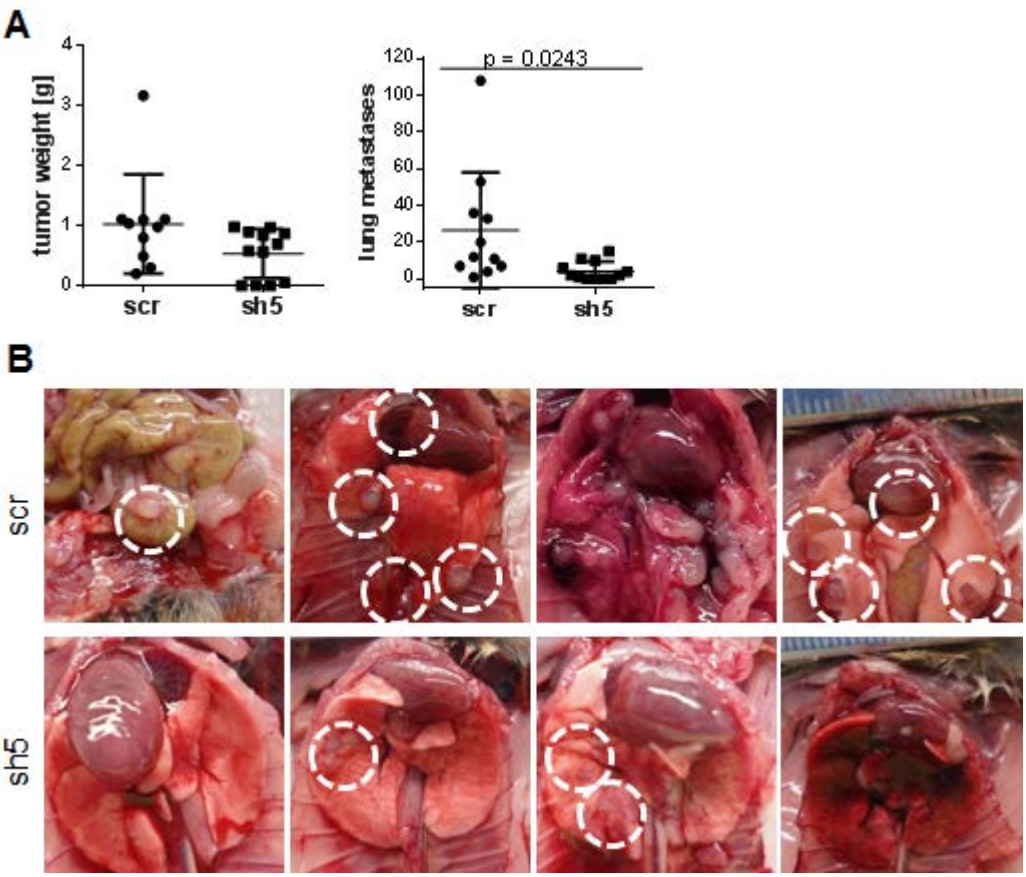

Fig. 11 Integrin β1 shRNA knockdown reduces metastases *in vivo.* (A) Mice injected with 344SQ Itgβ1 shRNA showed a significant reduction in the number of lung metastases. (B) Control mice showed distant metastases (e.g. intestines, heart), which were absent in the shRNA mice.

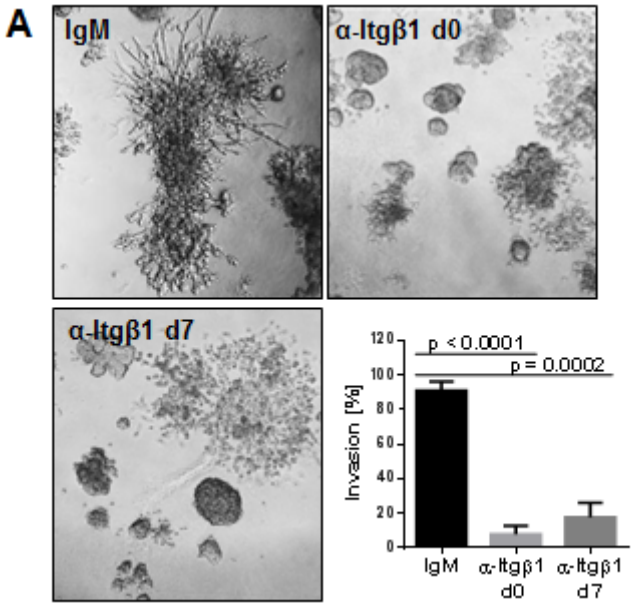

Fig. 12 Integrin β1 inhibition blocks 3D invasion in human mesenchymal cell lines. (A) H157 cells grown in 1. 5 mg/ml Matrigel/collagen I and treated with an ITGβ1-blocking antibody from day 0 or day 7 or IgM control. 90 structures were scored for invasiveness.

decreased Zeb1 and N-cadherin levels and a decreased downstream activation of the FAK/Src pathway (Fig. 13A & B). This effect was also observed upon miR-200ab induction in H157 wild-type cells (Fig. 14B), which also causes a decrease in the formation of invasive cell protrusions (Fig. 14A). This 3D phenotype was resembled in the cells treated with the Itgβ1-blocking antibody (Fig. 12A). Furthermore, the Itgβ1-knockdown cells had a more epithelial morphology (Fig. 14C) and decreased invasion in Transwell assays (Fig. 15B). In 3D Matrigel/collagen I cultures the control cells displayed a growth advantage versus the Itgβ1 knockdown cells and were significantly more invasive. Interestingly, despite normal growth in 2D culture the shRNA84 Itgβ1 KD cells were unable to survive in 3D culture (Fig. 15A). This result suggests that the Itgβ1-collagen I interaction mediates pro-growth/survival and pro-invasive signaling.

Invasion of the mesenchymal cells is dependent on FAK/Src pathway activation.

Given the observed FAK/Src pathway activation, we sought to study the importance of this pathway downstream of Itgβ1-matrix interactions in our murine cell line panel. Western Blot analysis showed significant activation of the FAK/Src pathway (including FAK, Src, paxillin, and cortactin) in the mesenchymal cells compared to the epithelial cells (Fig. 16A), along with increased phospho and total CRKL expression. Moreover, in the genetically manipulated 393P cells we observed an inverse correlation between the activation of this pathway, CRKL expression and the miR-200 levels (Fig. 16B). Inhibition of FAK with the reversible inhibitor, Y15

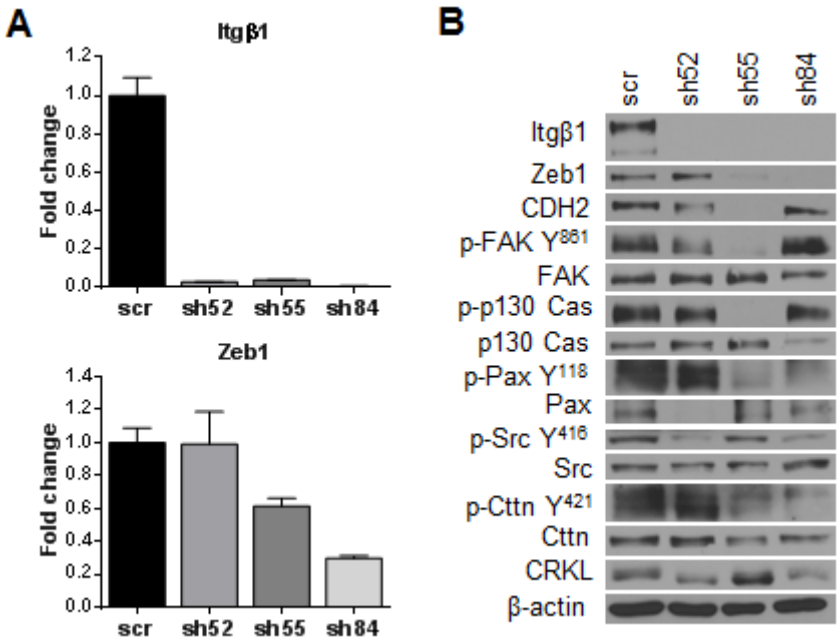

Fig. 13 Integrin β1 knockdown in human H157 cells. (A) Quantitative RT-PCR and (B) Western Blot analysis of H157 cells after Itgβ1-shRNA knockdown shows a partial MET.

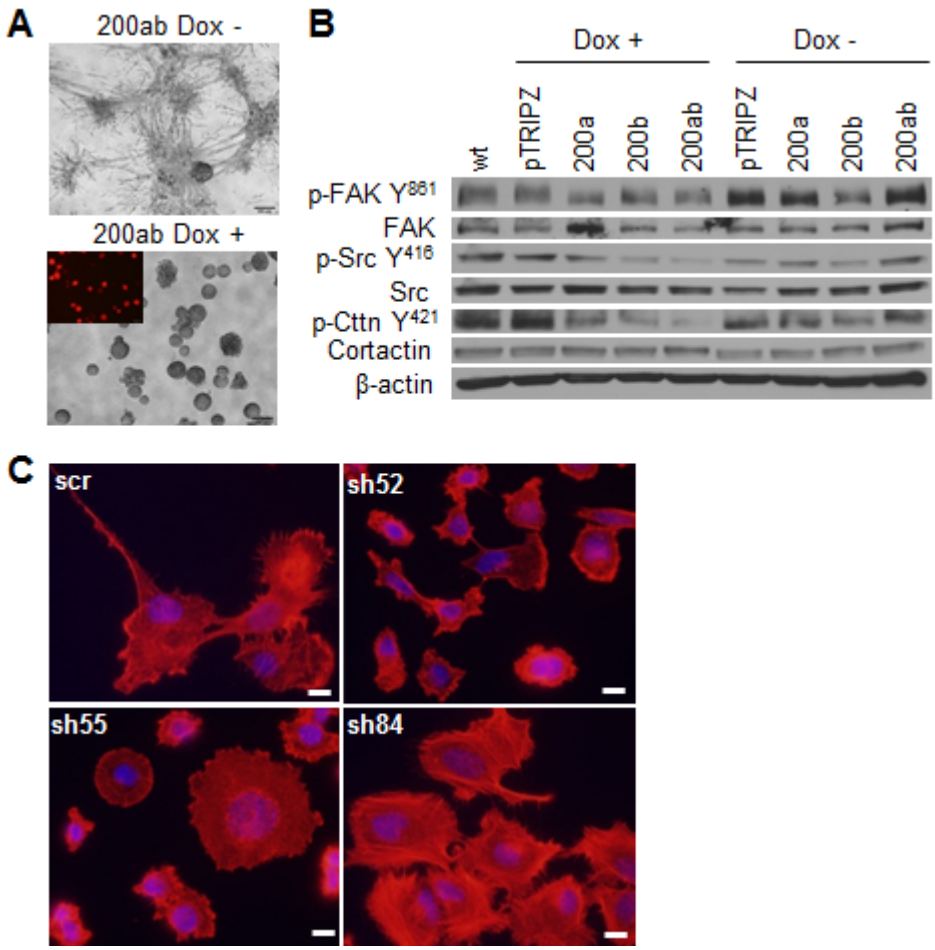

Fig. 14 MiR-200 re-expression and Integrin β1 knockdown in H157 cells cause an MET. (A) H157 cells grown in 3D culture (Matrigel/collagen mixture) for 11 days. (B) Western Blot analysis of the FAK/Src pathway of H157 cells after induction of miR-200. (C) H157 Itgβ1 knockdown cells stained for F-actin with Phalloidin and DAPI for the nucleus. Scale bar is 200 μm.

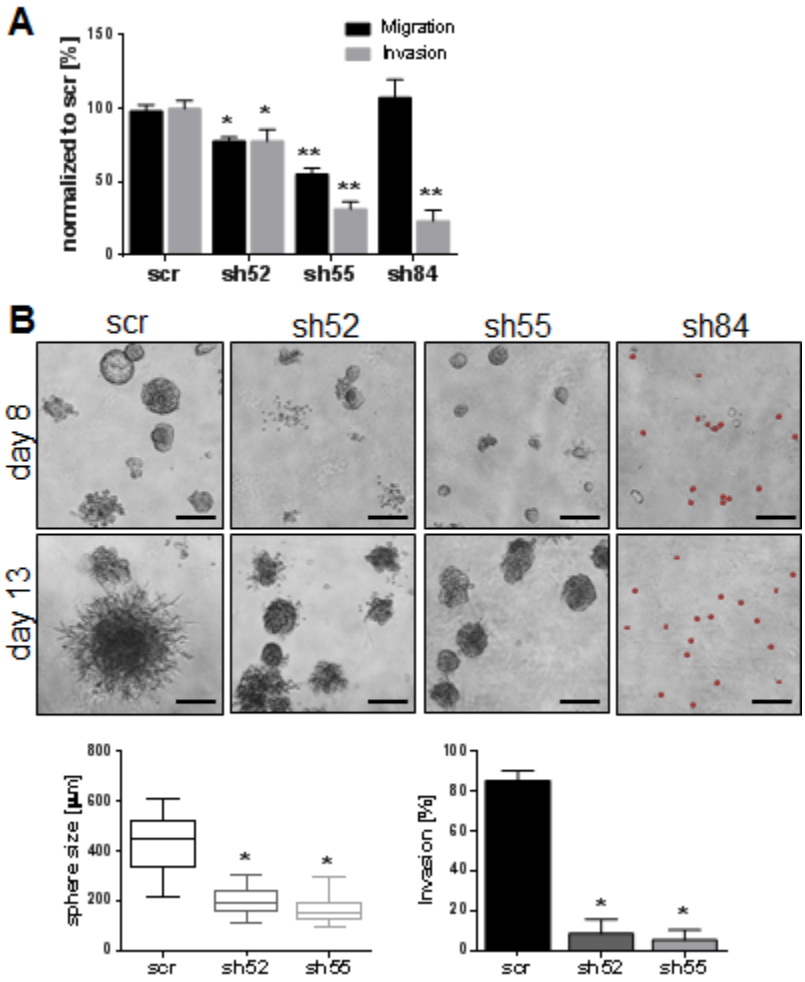

Fig. 15 Integrin β1-collagen I contact is necessary for H157 survival. (A) In vitro migration and assay for the Itgβ1 shRNA cells. * $p < 0.001$, ** $p < 0.0001$ (B) ITGβ1-knockdown cells grown on Matrigel/collagen I for 13 days and analyzed for sphere size and invasiveness. Cells for sh84 are pseudo colored and not included in graphical analysis due to phenotype. Scale bar is 200 µm. * $p \leq 0.0001$

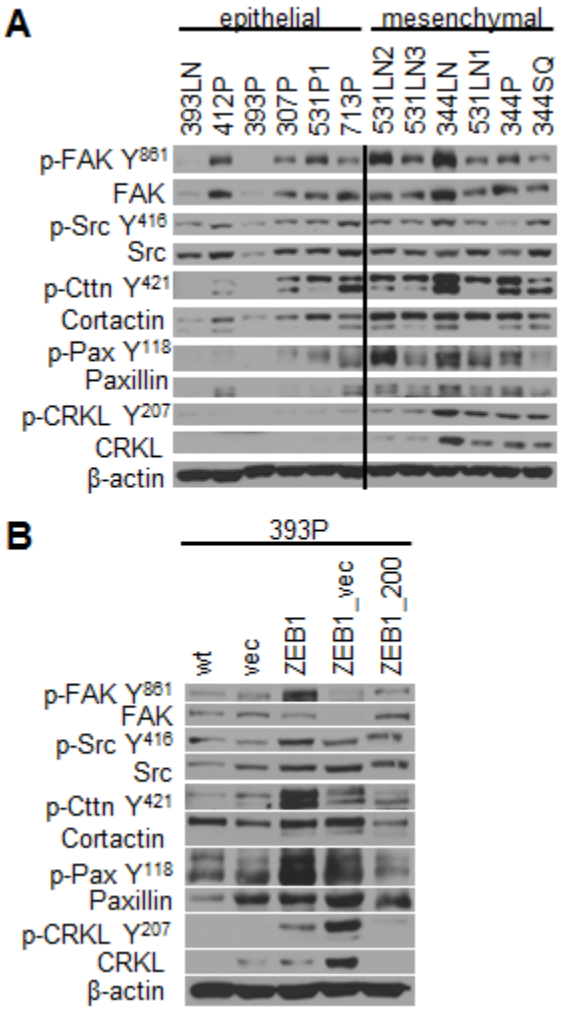

Fig. 16 The FAK/Src pathway is activated in mesenchymal cell lines. (A) Western Blot analysis shows increased FAK/Src/Cortactin pathway activation in the mesenchymal cells lines of the murine cell line panel and in cell lines stably expressing Zeb1 (B).

(Fig. 17A), significantly decreased 2D migration and invasion (Fig. 17B), and disassembly of pre-formed invasive cell protrusions in 3D 393P_ZEB1 cultures within 72 hrs (Fig. 17C). This disassembly was due to decreased cell adhesion as seen in a cell adhesion assay in which pre-treated cells were grown on different matrices (Fig. 18A). Cells that received continuous Y15 treatment showed a decreased ability to adhere, but removal of the inhibitor at the time of plating revealed that this effect was reversible (rather than a consequence of cell death). Taken together these results reveal that Itgβ1-mediated invasion is dependent upon FAK signaling.

Mesenchymal cell invasion is mediated through activated Src signaling.

The tyrosine kinase Src is known to interact with activated FAK, producing additional FAK phosphorylation at the tyrosine residues Y576/577, Y861 and Y925, as observed upon ZEB1 expression in the 393P cells (Fig. 19A). To further study the importance of the FAK/Src pathway in regulating invasion, we assayed the effect of the Src tyrosine kinase inhibitor, dasatinib. Dasatinib treatment blocked FAK activation (Fig. 19A) and significantly reduced 2D migration and invasion, suppressing the highly invasive 393P_ZEB1 cells to the baseline control levels (Fig. 19B). Dasatinib treatment in 3D assays blocked FAK/Src signaling (Fig. 20C), and inhibited the collagen I-dependent invasion of the mesenchymal 393P_ZEB1 cells (Fig. 20A & B). Moreover, combination treatment of dasatinib with an Itgβ3-blocking antibody phenocopied the combined Itgβ3/Itgβ1-blocking antibody treatment (Fig. 21 A and B). To rule out off targets effects of dasatinib, we used the tyrosine

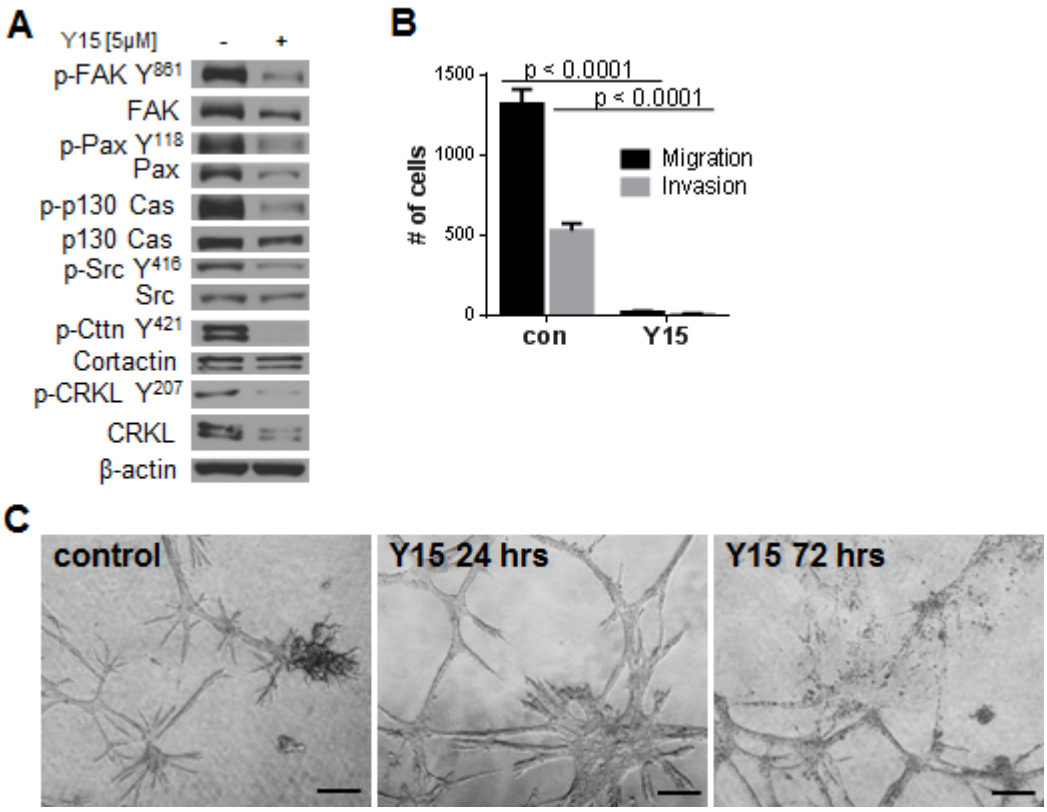

Fig. 17 The FAK/Src pathway is activated in mesenchymal cell lines and required for cell invasion. (A) FAK/Src/Cortactin pathway activation in the mesenchymal cells lines is inhibited upon a 24 hr treatment with a FAK inhibitor (Y15). (B) In vitro migration and invasion assay of 393P_ZEB1 cells treated with Y15 (5 μM). (C) FAK inhibition of 393P_ZEB1 cells in Matrigel/collagen I causes the disassembly of cell protrusions (day 7 pictures). Scale bar is 200 μm.

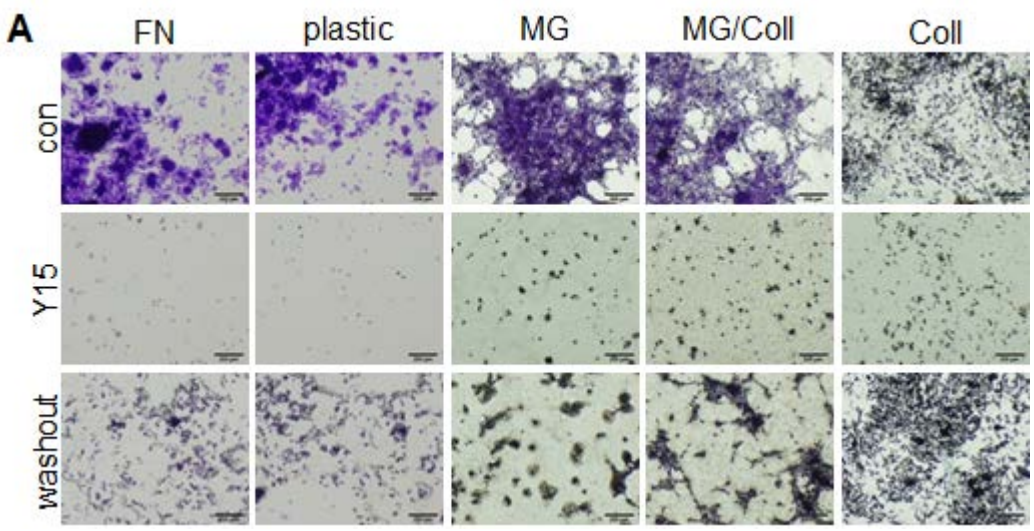

Fig. 18 Treatment with the FAK inhibitor affects cell adhesion and is reversible. (A) 393P_ZEB1 cells pre-treated with the FAK inhibitor Y15 (5μM) for 24 hrs before plated on the different matrices as indicated (FN: Fibronectin, MG: Matrigel, Coll: collagen type I). Cells were fixed and stained after 7 hrs post plating.

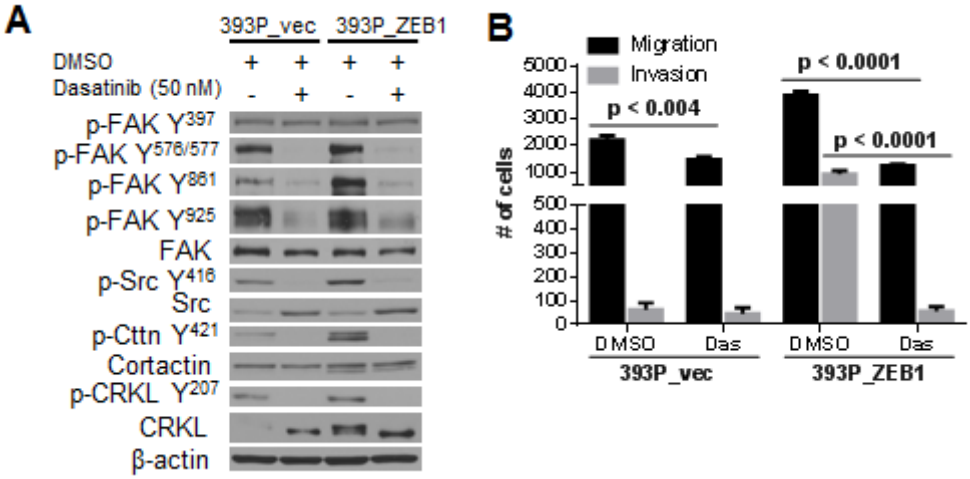

Fig. 19 Invasion of the mesenchymal cells is mediated through activated Src signaling. (A) Western Blot analysis of 393P_ZEB1 and control cells after dasatinib treatment for 7 hrs. (B) Dasatinib treatment inhibits the migratory and invasive ability of mesenchymal cells in Transwell assays.

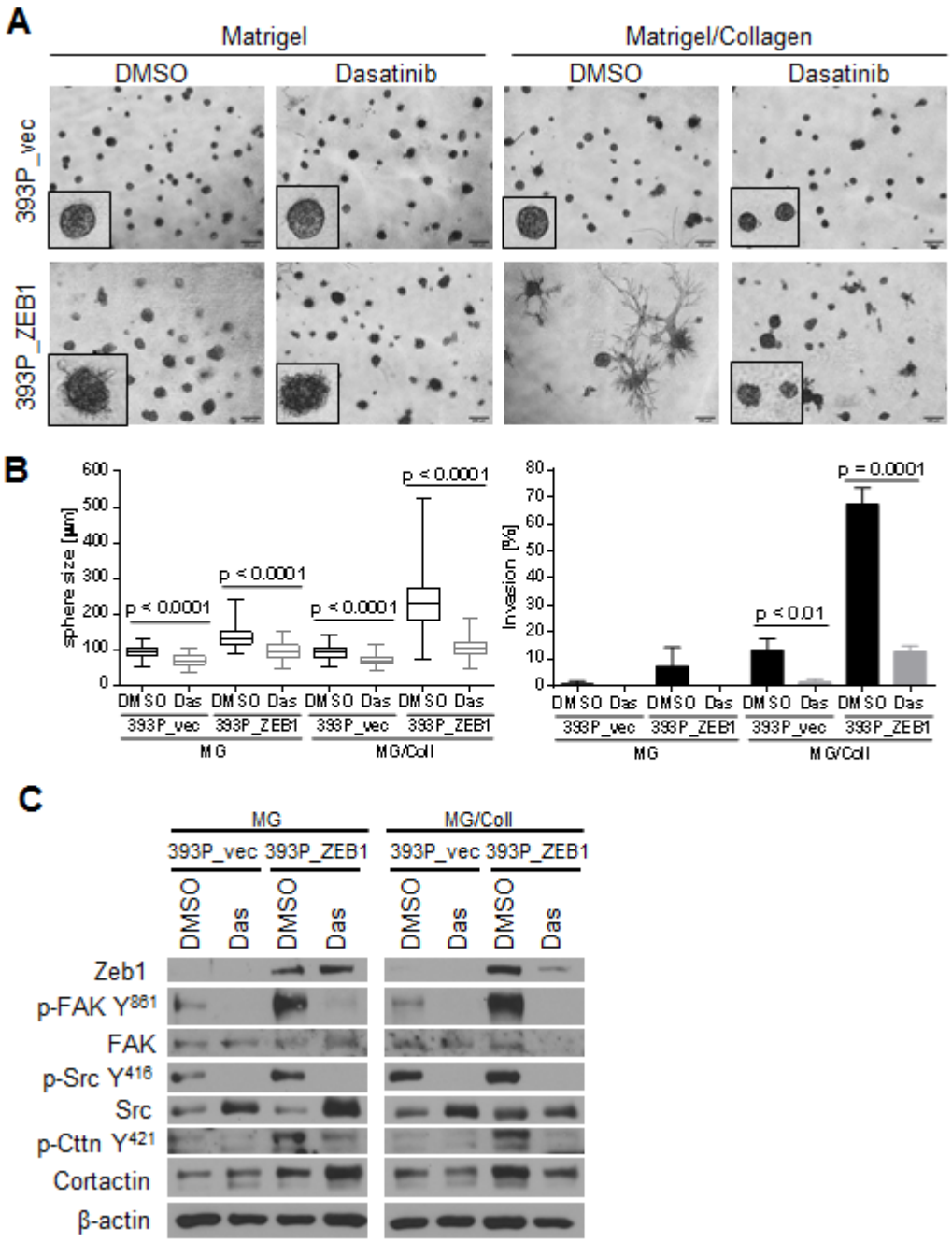

Fig. 20 3D invasion of the mesenchymal cells is mediated through activated Src signaling and substrate dependent. (A) 393P_Zeb1 and control cells grown in 3D cultures. Invasion of 393P_Zeb1 cells in a mixture of Matrigel/collagen I (1.75 mg/ml) is inhibited upon dasatinib treatment (50 nM). Images were taken at day 7 after a 3 day treatment. (B) Quantification of sphere size and invasiveness of cells in 3D cultures from (A). Represented is the average of 3 wells, each measuring 30 structures in size and scoring 50 structures for invasiveness. (C) Western Blot analysis of cells grown in 3D from (A) after dasatinib treatment.

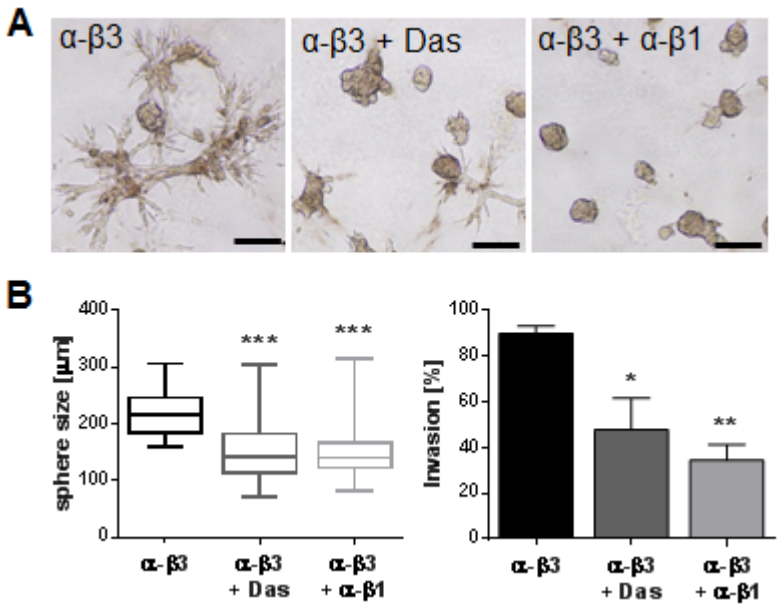

Fig. 21 Dasatinib treatment mimics the Integrin β1 phenotype in 3D assays. (A) 393P_ZEB1 cells grown on Matrigel/collagen and treated with Itgβ3 blocking-antibody alone or in combination with dasatinib or an Itgβ1 blocking-antibody (combined treatment started day 4). (B) Images and quantification of sphere size and invasion were taken at day 7. Scale bar is 200 µm. * $p < 0.007$, ** $p = 0.0002$, *** $p < 0.0001$.

kinase inhibitor Imatinib in 3D studies, which targets the same kinases as dasatinib except for Src. Imatinib treatment, either started at day 0 or day 4 did not inhibit invasion (Fig. 22A and B). Dasatinib treatment of human H157 cells blocked Src pathway activation, suppressing Transwell migration and invasion (Fig. 23A & B), and causing the cells in 3D culture to remain as single cells or tiny clusters when added at day 0 (Fig. 23C). Treatment with dasatinib at later time points disrupted the invasive structures, mimicking the miR-200 phenotype (Fig. 23C bottom row and Fig. 24A). We further investigated the role of the ECM by comparing cells grown in monolayer culture to cells grown in suspension (Fig. 24B), which showed FAK/Src pathway deactivation in cells grown in suspension. These results demonstrate that the FAK/Src pathway activation is driven by the ECM composition and required for the mesenchymal cell invasion.

In addition to the pharmacological inhibition of Src we utilized a genetic approach by using either a dominant-active (Y527F, DA) or dominant-negative (K295R, DN) form of Src. The DA Src was introduced into the epithelial 393P and 412P cells, which showed an increase in activated Src (Fig. 25A) and a slight morphology change in the 393P cells (Fig. 25B), yet without any functional phenotype (Fig. 25C). In the 412P cells, the DA Src caused a decrease in migration (Fig. 25C), opposite to our expectations. The DN form of Src introduced in the highly invasive 344SQ, 531LN2 and 344LN cells did not inhibit Src activation as expected by protein levels (Fig. 25D) nor was any morphology change (Fig. 25E) observed, but rather led to an increase in phospho-Src levels which correlated with an increase in Transwell migration and invasion (Fig. 25F). Those controversial

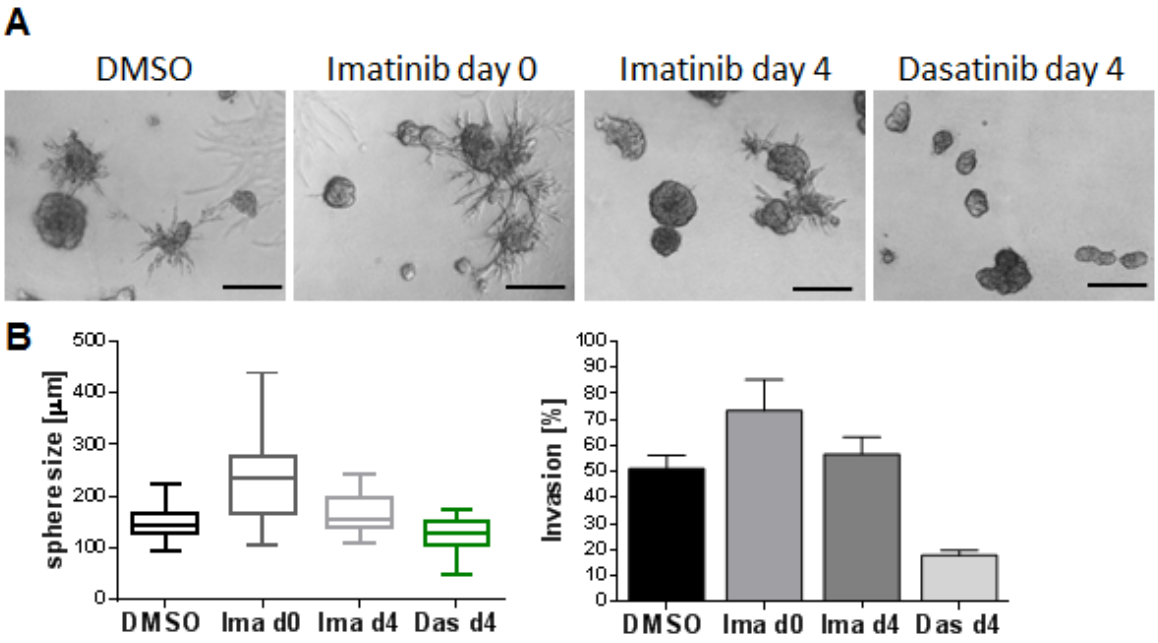

Fig. 22 Invasion of the mesenchymal cells is Src dependent. (A) Invasion of 393P_Zeb1 cells grown in a mixture of Matrigel/collagen I (1.75 mg/ml) is not inhibited upon treatment with Imatinib (1 µM) compared to dasatinib (50 nM) treatment. Images were taken at day 7. Scale bar is 200 µm. (B) Sphere size and invasion represent the average of 3 wells with 30 structures quantified in each.

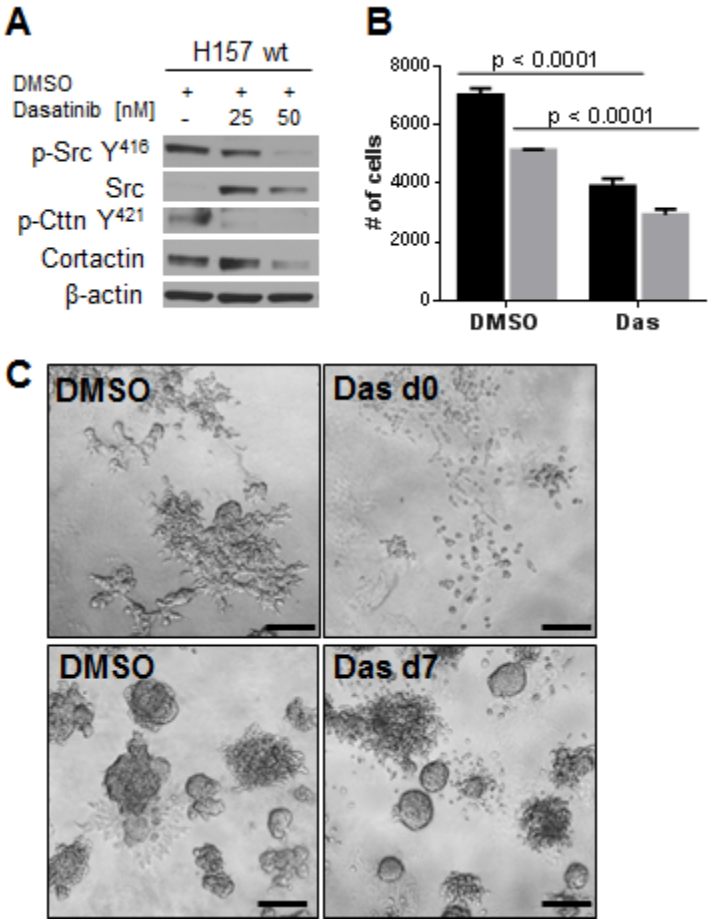

Fig. 23 Invasion of the human mesenchymal cells is mediated through activated Src signaling. (A) Western Blot analysis of H157 cells treated for 24 hrs with the dasatinib at 25 and 50 nM. (B) In vitro migration (black bar) and invasion (grey bar) assay of H157 cells treated with dasatinib (50 nM). (C) H157 cells grown in Matrigel/collagen I and treated with dasatinib starting at day 0 (pictures represent day 9).

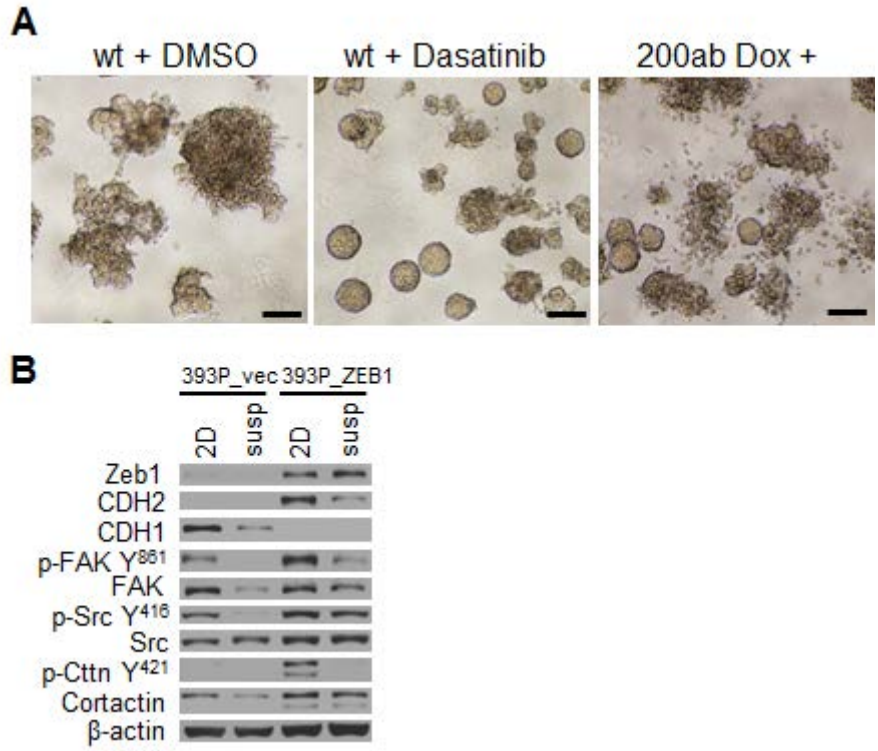

Fig. 24 Dasatinib treatment mimics the Integrin β1 and miR-200 phenotype in 3D assays. (A) H157 wild type and H157_200ab grown in 3D Matrigel/collagen. Dasatinib or vehicle were added at day 7. Images represent day 11. Scale bar is 200 μm. (B) Activation of the FAK/Src pathway is substrate dependent as seen in comparing cells grown on a petridish vs. suspension cells grown on low adhesion culture plates for 7 days.

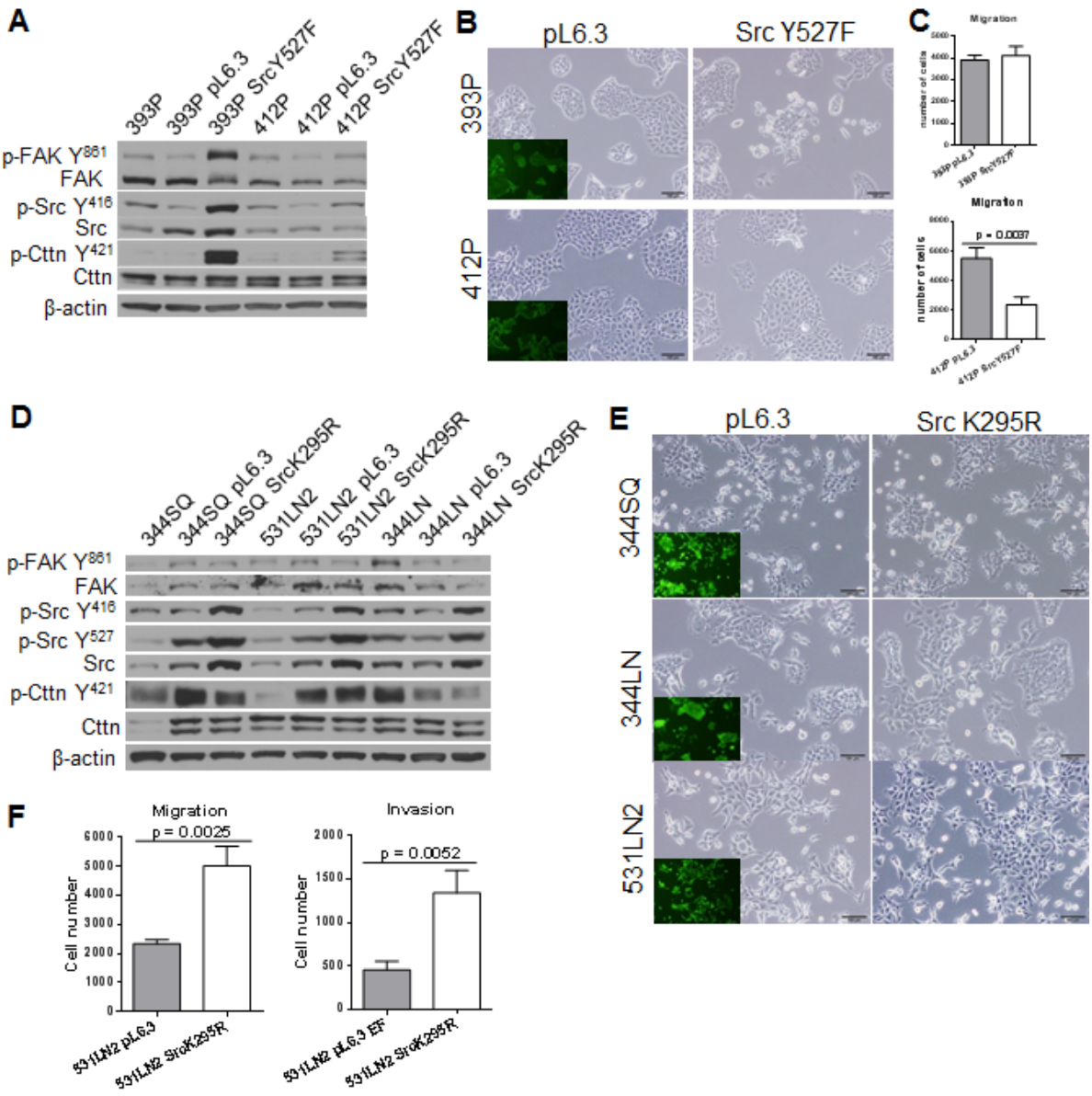

Fig. 25 Dominant active (Y527F) and dominant negative (K295R) Src. (A) Western Blot analysis and morphology (B) of 393P and 412P cells infected with DA Src. (C) Migration of 393P and 412P cells with Csk. (D) Western Blot analysis and morphology (E) of 344SQ, 531LN2 and 344LN cells infected with DN Src.(F) Migration and invasion of 531LN2 cells is increased with Csk.

results could be explained by a possible compensation of other Src- family kinase (SFK) members. We therefore used another approach to inhibit the SFK members by infecting the cells with the SFK negative regulator Csk [26]. Infection of the highly invasive 393P_ZEB1 cells with Csk (with or without a GFP-tag) resulted in an increase in Csk mRNA and protein levels after induction with Doxycycline (Fig. 26A and B), yet no decrease in Src activation was observed (Fig. 26B). Alterations in Csk levels have been shown to affect the cytoskeleton and the ability of cells to adhere to fibronectin, neither of which showed an effect in the infected cells (Fig. 26C and D) [43]. Furthermore, growth of the Csk overexpressing cells did not show a phenotype in a 3D Matrigel/collagen I matrix (Fig. 26E).

Src inhibition blocks TGFβ-induced EMT and *in vivo* metastasis.

TGFβ is a well-known EMT inducer to which we have previously shown the metastasis-prone KP cells are quite sensitive [16]. We next asked if Src inhibition would block the TGFβ-induced EMT in 344SQ or 531LN2 cells. In addition to dasatinib, the more specific Src inhibitor AZD0530, blocked Src pathway activation even in combination treatment with TGFβ (Fig. 27A). Interestingly, combined treatment with AZD0530 showed a decrease of Zeb1, which was reflected in the cellular morphology. Cells treated with TGFβ alone showed a fibroblastic phenotype, whereas cells that received TGFβ and AZD0530 displayed an epithelial morphology (Fig. 27B). Similar to the results with the invasive 393P_ZEB1 cells, treatment with either Src inhibitor decreased Transwell migration and invasion of the mesenchymal

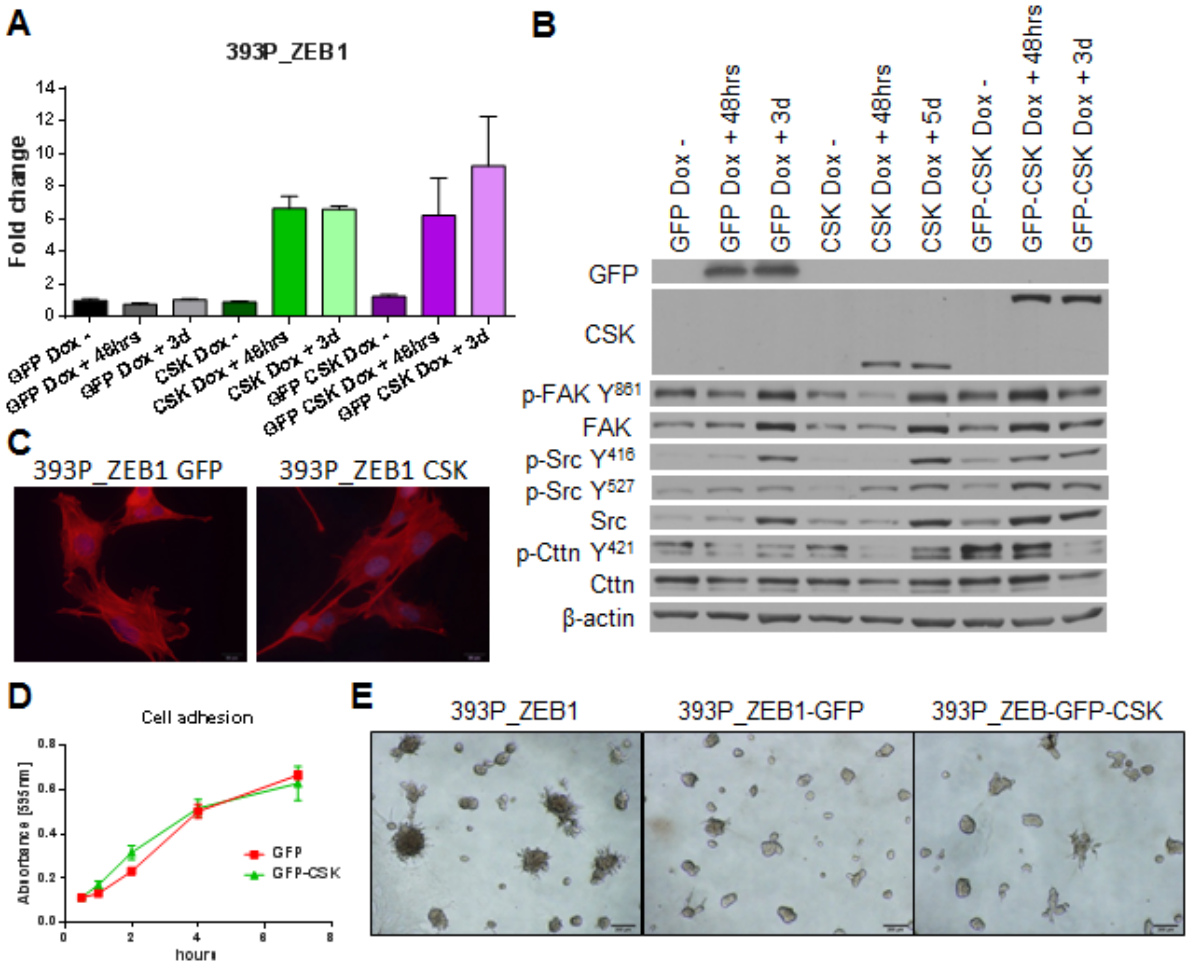

Fig. 26 393P_ZEB1 cells infected with Csk. (A) mRNA and (B) protein levels of 393P_ZEB1 cells infected with Csk or GFP-Csk after induction with Dox. (C) 393P_ZEB1 cells infected with Csk grown on gelatin and stained for F-actin and DAPI. (D) Quantification of adhesion of the infected cells on Fibronectin at the indicated time points. (E) Csk does not affect invasion of 393P_ZEB1 cells in 3D Matrigel/collagen I.

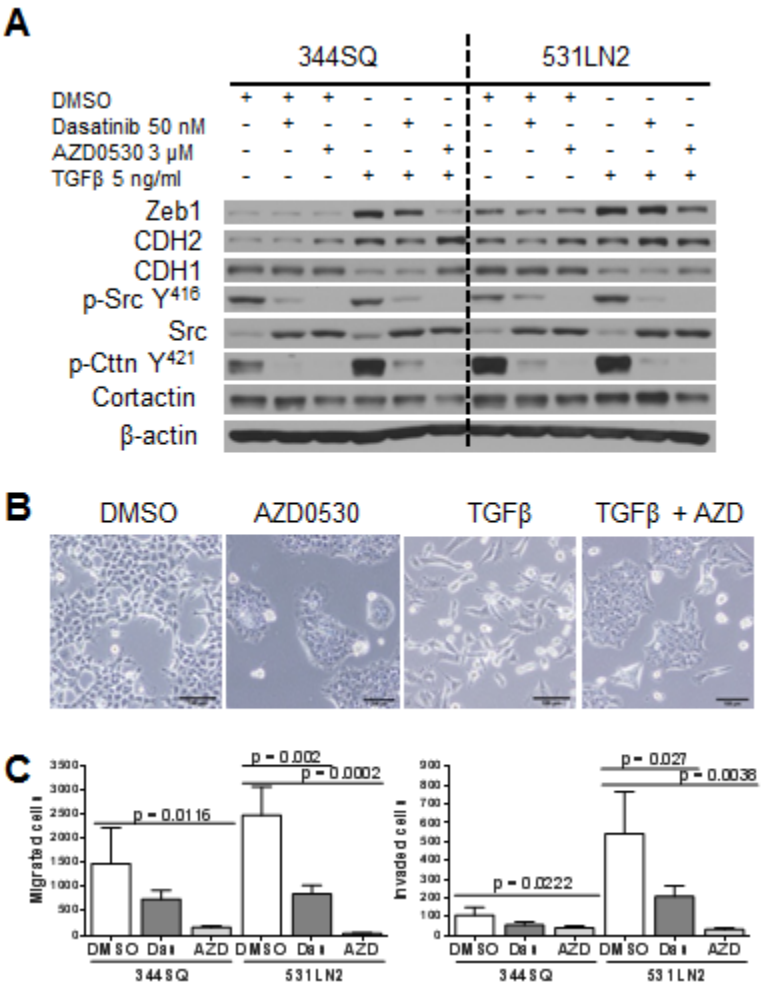

Fig. 27 Migration, invasion & TGFβ response of 344SQ and 531LN2 cells are blocked with Src inhibitors. (A) Western Blot analysis of 344SQ and 531LN2 cells treated with Src inhibitors and TGFβ at the indicated concentrations for 3 days. (B) Morphology of the 344SQ cells in the indicated treatment conditions. (C) The migratory and invasive Transwell assays upon DMSO, dasatinib (50 nM) or AZD0530 (3 μM) treatment.

344SQ and 531LN2 cells (Fig. 27C). In 3D culture, treatment of 344SQ cells with TGFβ caused the spheres to hyper-proliferate and become highly invasive (Fig. 28A, left column), as reported [16]. Combined treatment with TGFβ and either of the Src inhibitors led to a significant reduction in sphere size and invasion, which was more pronounced with AZD0530 (Fig. 28A & B).

The 344SQ cells are paradigmatic of the highly metastatic KP cells in our syngeneic murine model [16]. To assess whether dasatinib blockade of the Src signaling pathway could suppress metastases, we injected syngeneic mice with 344SQ cells and dosed them with 10 or 20 mg/kg dasatinib 5 days/week. The results show that treatment at either concentration significantly reduced the number of lung metastases (Fig. 29A). Moreover, metastases were found in the liver, kidneys, spleen, intestines and diaphragm in the control mice but not in the treated mice (Fig. 29B). Immunohistochemical staining of the subcutaneous tumors demonstrated a strong correlation between p-Src and the number of metastases (Fig. 29C), with the highest number of metastases found in mice with the highest intratumoral p-Src levels.

CRKL is a miR-200 target that mediates integrin-dependent signaling.

In order to identify the underlying mechanism of how miR-200 regulates the Integrin-FAK/Src pathway, we performed a qPCR screen of several integrin signaling adaptors in our murine cell lines with altered miR-200 expression levels (Fig. 30A and B). Integrin adaptors have been implicated in many cancer types due to their importance in transmitting signals from the ECM to intracellular signaling

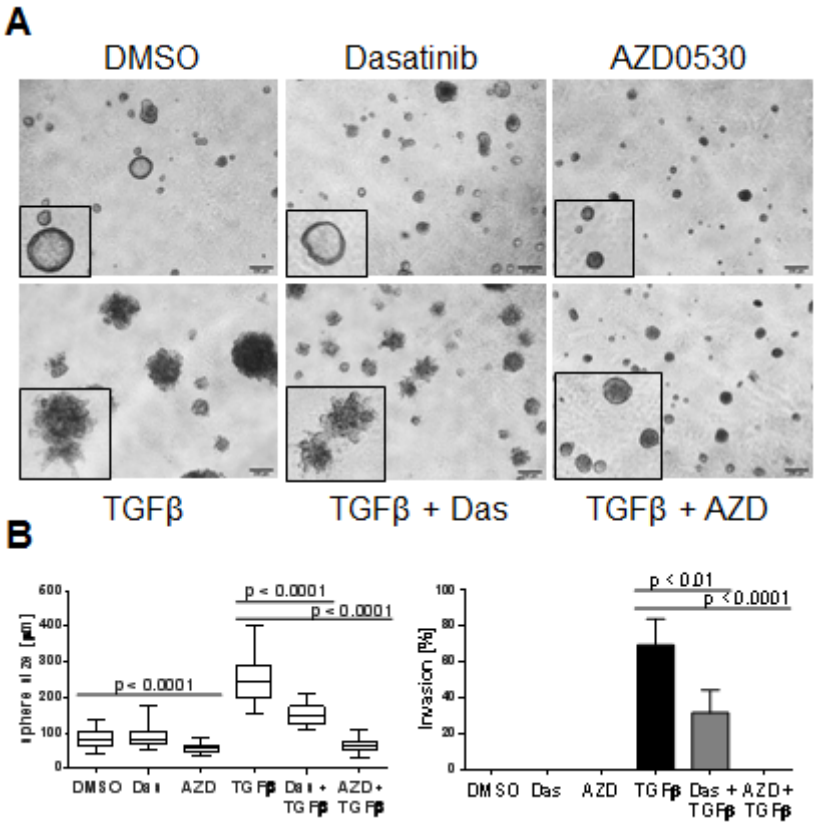

Fig. 28 Migration, invasion & TGFβ response of 344SQ and 531LN2 cells are blocked with Src inhibitors. (A) Sphere formation of 344SQ in 3D Matrigel cultures. Images were taken at day 10 and sphere size and invasiveness scored (B). Dasatinib (50 nM) was added at day 4, AZD0530 (3 μM) at day 5 and TGFβ (5 ng/ml) at day 6.

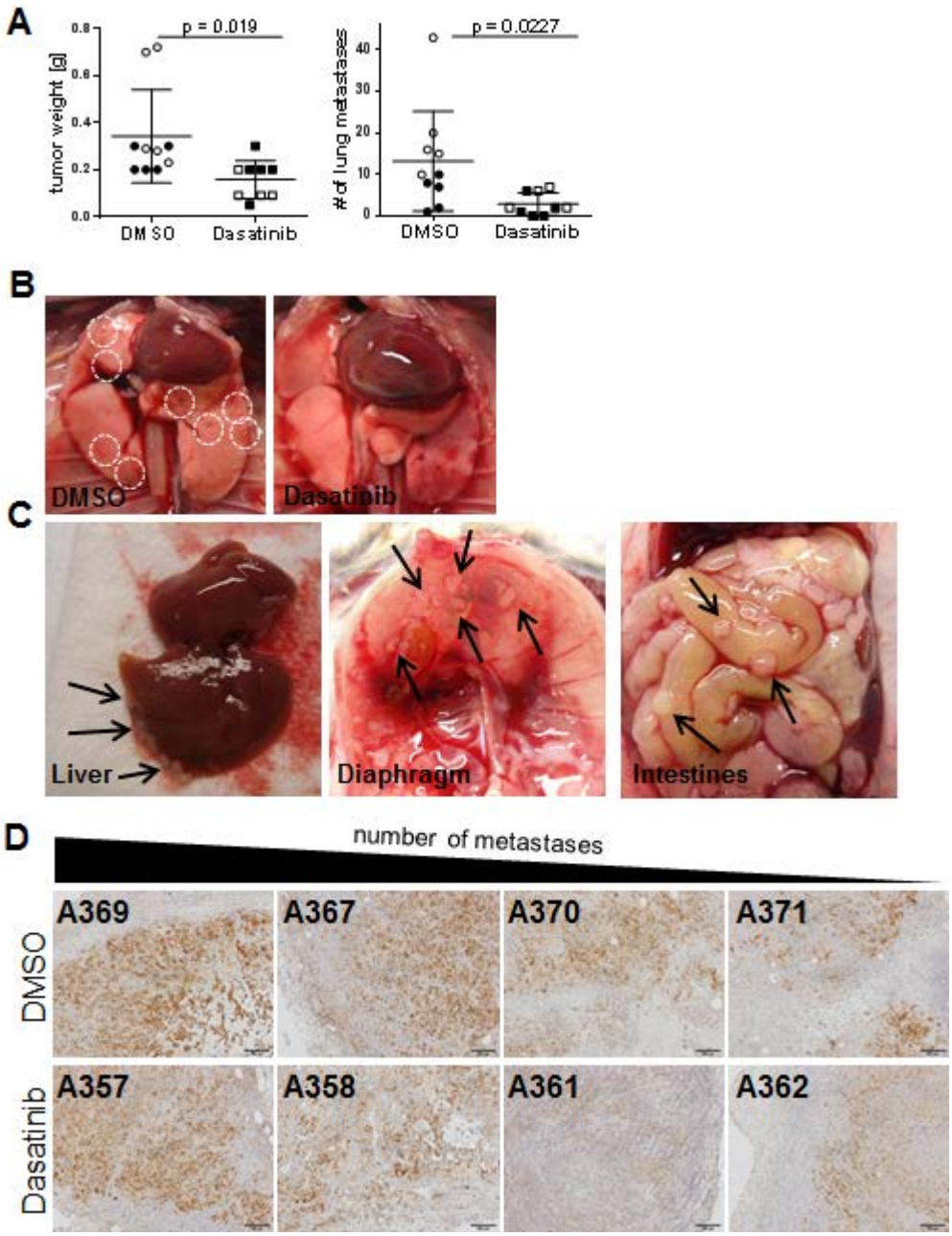

Fig. 29 Dasatinib treatment *in vivo* affects metastases and phospho-Src expression. (A) Primary tumor weight and number of lung metastases in syngeneic mice treated with dasatinib n=9 (10 mg/kg: solid shapes, 20 mg/kg: empty shapes) or vehicle n=10. (B) Lung metastases in the control and treated mice. (C) Distant organ metastases found in the control mice (DMSO) as indicated by the black arrows. (D) Immunohistochemistry of subcutaneous tumors from dasatinib treated or control mice stained for p-Src Y418. The left 2 columns represent mice with a high number of metastases, the right 2 columns mice with few or no metastases.

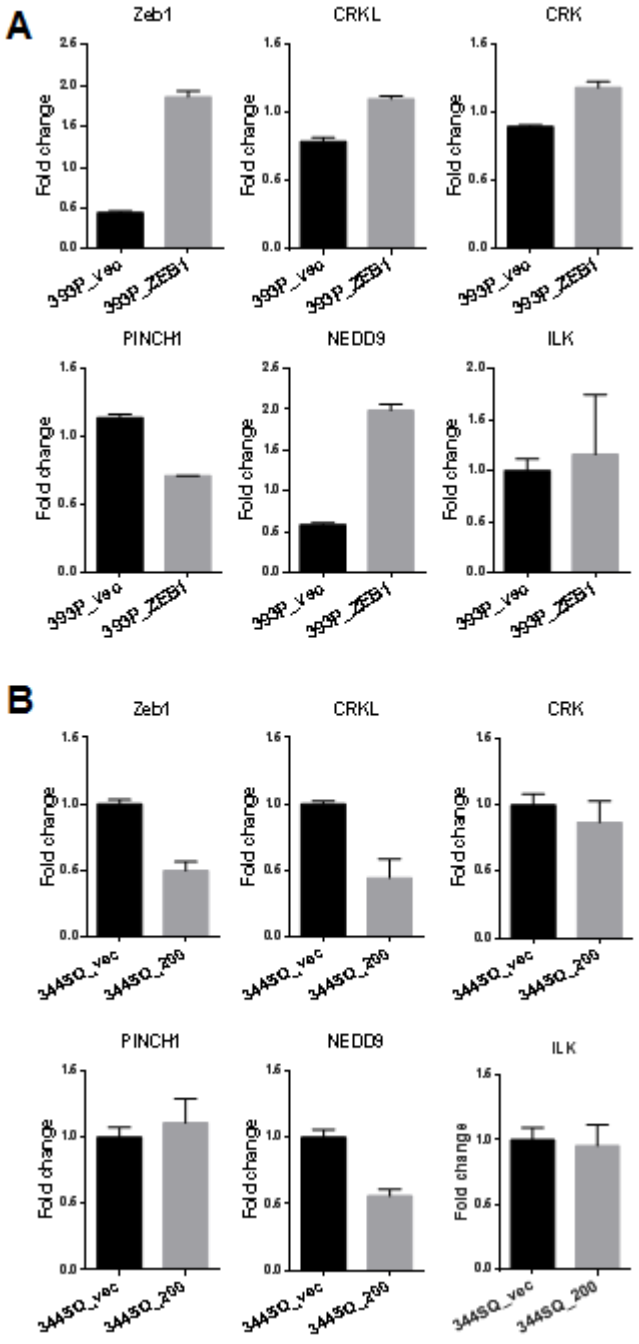

Fig. 30 mRNA expression of integrin adaptor molecules in the murine cell lines. Quantitative RT-PCR analysis in the 393P_ZEB1 vs. control cells (A) and 344SQ_200 vs. control cells (B).

pathways by acting as a central hub [33]. From this screen we identified CRKL, which inversely correlated with the miR-200 levels. CRKL has been identified as an oncogene in NSCLC and its overexpression correlates with poor prognosis [36, 38]. As an integrin adaptor molecule it plays an important role as a scaffold protein, leading to integrin-dependent complex formation especially at sites of focal adhesions. Its protein expression in the ltgβ1 knockdown cells (Fig. 13B), the murine cell line panel as stratified by EMT status (Fig. 16A & B) and after treatment with FAK (Fig. 17A) or Src inhibitors (Fig. 19A) suggested a potential role for CRKL in coupling the ECM-integrin signals to the FAK/Src pathway.

CRKL is a potential miR-200 target, with two predicted target sites in the 3' untranslated region (Fig. 31A). To test whether total CRKL levels are regulated by miR-200, and could therefore regulate signaling downstream of ltgβ1, we constructed a luciferase reporter containing the CRKL 3' untranslated region (UTR). The luciferase reporter assay confirmed that wild-type CRKL is a direct miR-200b and -c target, with mutation of the second predicted seed sequence or both together reversing the effect of pre-miR binding (Fig. 31B-D). Functionally, siRNA knockdown of CRKL reduced *in vitro* migration and invasion of H157 cells in Transwell assays (Fig. 32A-C) and 3D Matrigel/collagen I cultures (Fig. 33A). The 3D structures displayed a more rounded morphology, which was further seen in the adhesion assay on fibronectin (Fig. 33B). Consistent with its role as an adaptor molecule, the effect of CRKL was mediated by blockade of FAK and Src localization to focal adhesion sites (Fig. 34A), rather than phosphorylation of the FAK/Src pathway.

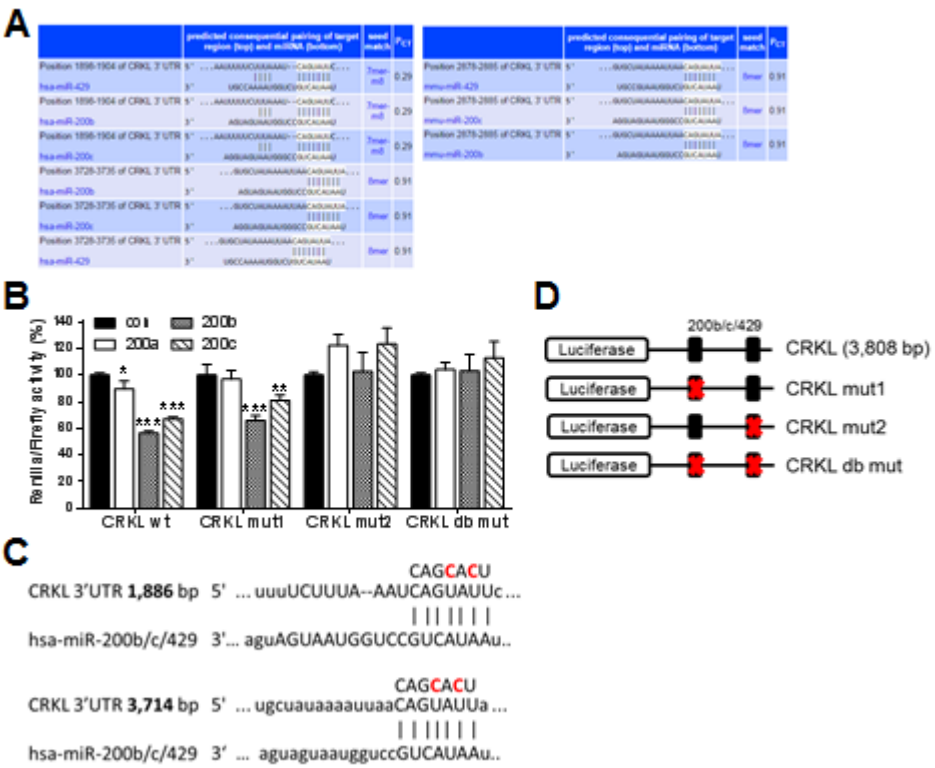

Fig. 31 CRKL is a direct miR-200 b and c target. (A) Prediction score of human and mouse CRKL being a miR-200 target using Targetscan. (B) Luciferase Reporter Assay in H157 cells using hRL_3' CRKL wt and mutant constructs. * $p < 0.05$, ** $p < 0.03$, *** $p < 0.003$ (C) The CRKL 3'UTR contains two predicted miR-200b/c/429 sites at the indicated locations. Two point mutations were introduced in each miR-200 seed sequence (red). (D) Four wt or mutant 3'UTR constructs were individually generated and cloned into the hRL vector.

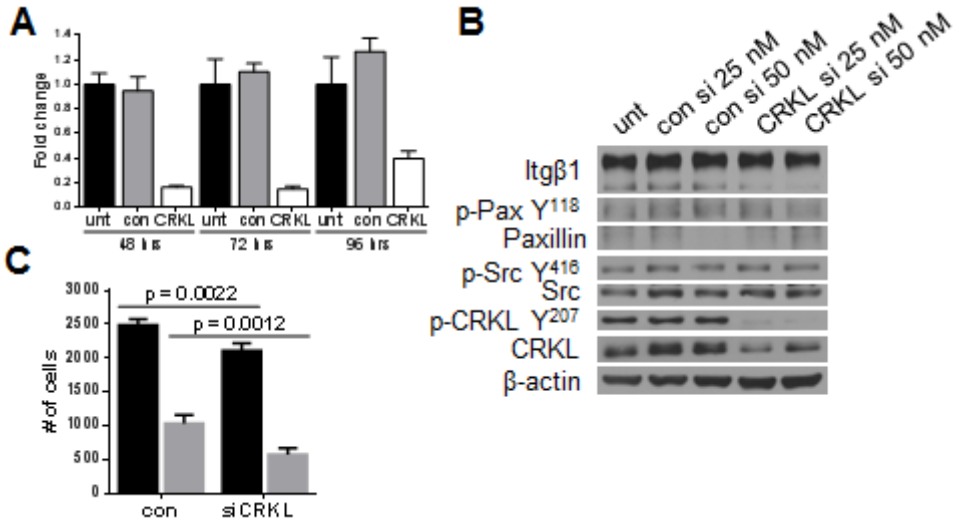

Fig. 32 CRKL siRNA transfection in H157 cells. (A) CRKL mRNA level after transfection with CRKL siRNA SMARTpool (final concentration 25 nM) compared to control siRNA and untreated cells. (B) Western Blot analysis of CRKL siRNA 48 hrs post-transfection using different siRNA concentrations. (C) Migration (black bar) and invasion (grey bar) of H157 cells using CRKL siRNA.

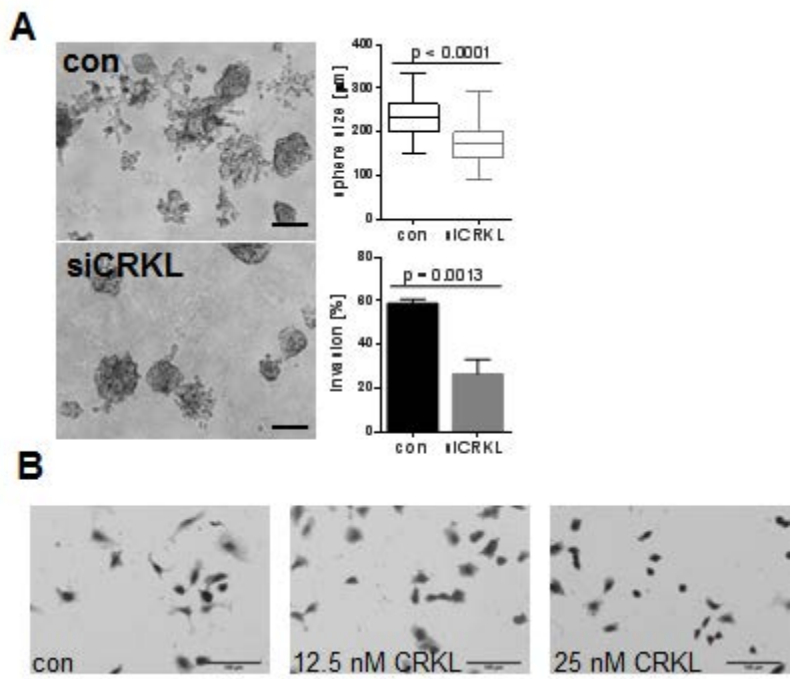

Fig. 33 CRKL siRNA affects 3D invasion and adhesion on Fibronectin (A) H157 transfected with CRKL siRNA (or control siRNA) grown in 3D Matrigel/collagen I (1.5 mg/ml) for 9 days. Scale bar is 200 µm. (B) Adhesion assay of H157 on Fibronectin transfected with CRKL siRNA.

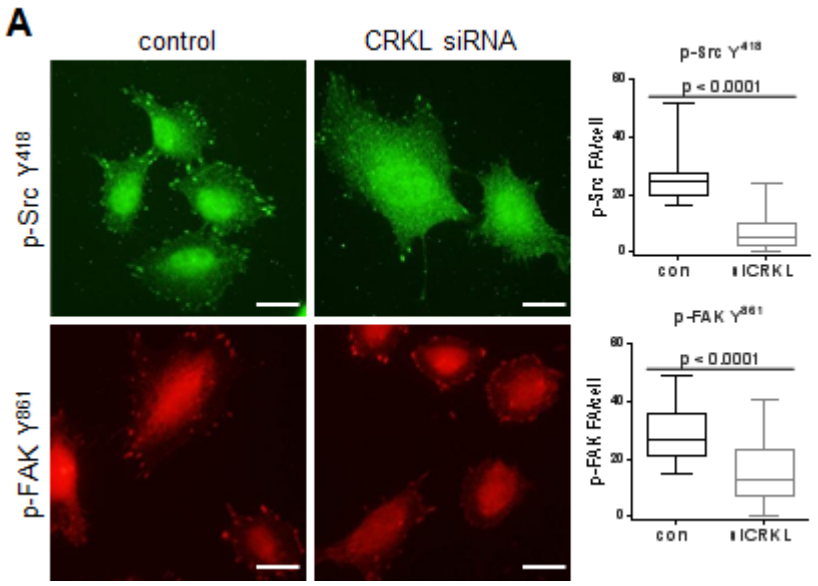

Fig. 34 CRKL knock-down affects localization of p-Src and p-FAK to focal adhesions. (A) Immunofluorescence staining of transfected H157 stained for p-Src Y418 or p-FAK Y861. An average of 30 cells was counted for positive staining at their focal adhesions (FA). Scale bar is 20 μm.

In addition to the CRKL siRNA, we used an shRNA-based knockdown approach in the mesenchymal 344SQ and 393P_ZEB1 cells. CRKL knockdown in the 344SQ cells (Fig. 35A) caused a significant decrease in the phospho-FAK and Src levels in shRNA 1 and 2 (Fig. 35B), which affected adhesion on a fibronectin matrix (Fig. 35C). Furthermore, the knockdown causes a functional decrease in Transwell migration and invasion (Fig. 36A) and a growth disadvantage in 3D assays in Matrigel (Fig. 36B). Similar results were obtained in the 393P_ZEB1 cells with CRKL knockdown (Fig. 37A), even though the effect on the FAK/Src pathway activation was not seen at the biochemical level (Fig. 37B), the functional consequences were the same as in the 344SQ cells (Fig. 37C, Fig. 38A and B). The effect on the localization of phospho-FAK and Src was confirmed biochemically, using a cytosolic and particulate separation approach. CRKL knockdown causes a defect in the localization/assembly of the activated FAK/Src complex, as seen by Western Blot analysis (Fig. 39A). Those results were further validated by immunofluorescent staining of p-Src and p-FAK, which are no longer localized at the focal adhesions (Fig. 40A, top 2 panels, and B). In addition, the focal adhesion marker Paxillin is mostly localized in the cytoplasm in the CRKL knockdown cells and there is no co-localization found of p-FAK and Paxillin at the focal adhesions compared to the control cells (Fig. 40A, lower panel, and B). This result confirms that CRKL is necessary for proper focal adhesion complex formation.

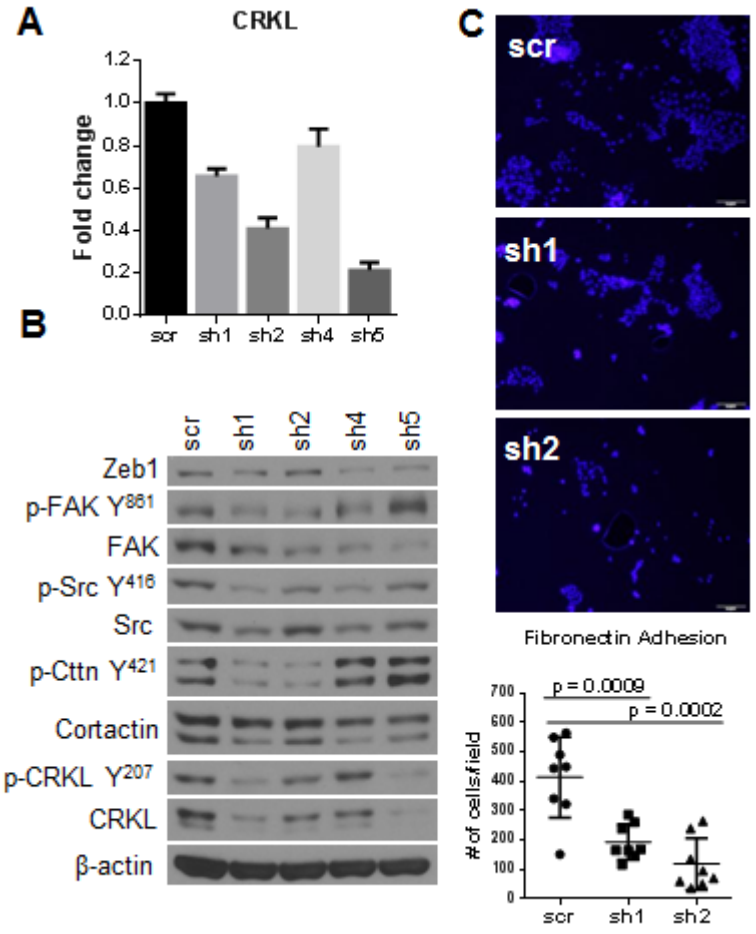

Fig. 35 CRKL knockdown in 344SQ cells causes a defect in adhesion. (A) Quantitative RT-PCR and (B) Western Blot analysis of 344SQ cells after CRKL-shRNA knockdown. (C) Adhesion of CRKL shRNA cells on Fibronectin shows a decrease compared to the control cells (cells stained with DAPI for the nucleus).

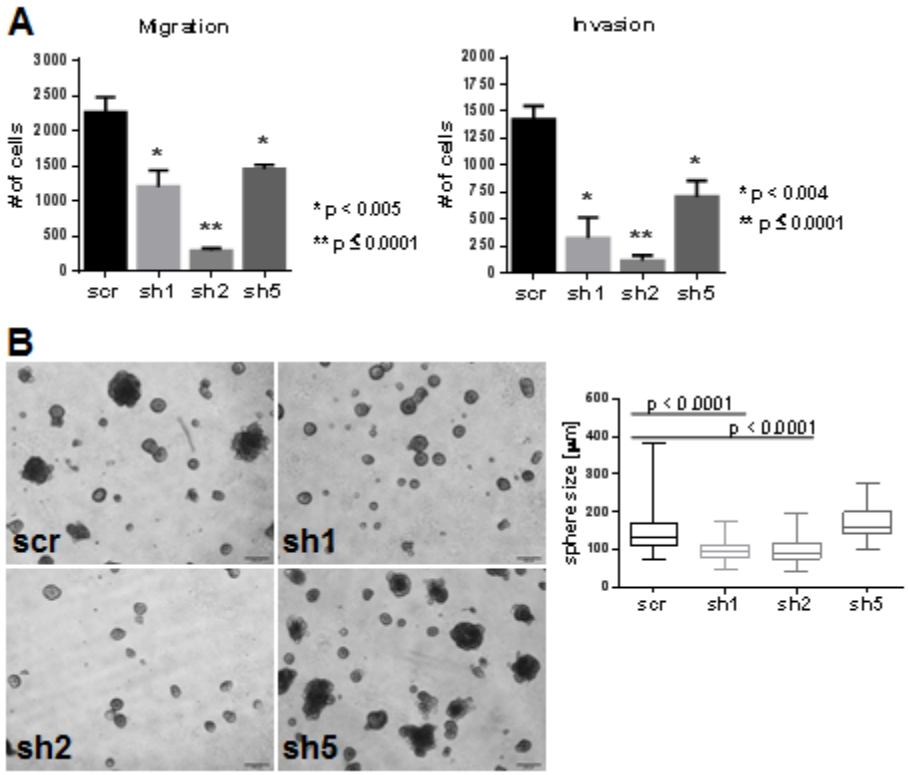

Fig. 36 CRKL knockdown in 344SQ cells causes a decrease in migration and invasion. (A) CRKL shRNA causes a significant decrease in Transwell migration and invasion. (B) CRKL knockdown causes a reduction of growth in 3D Matrigel.

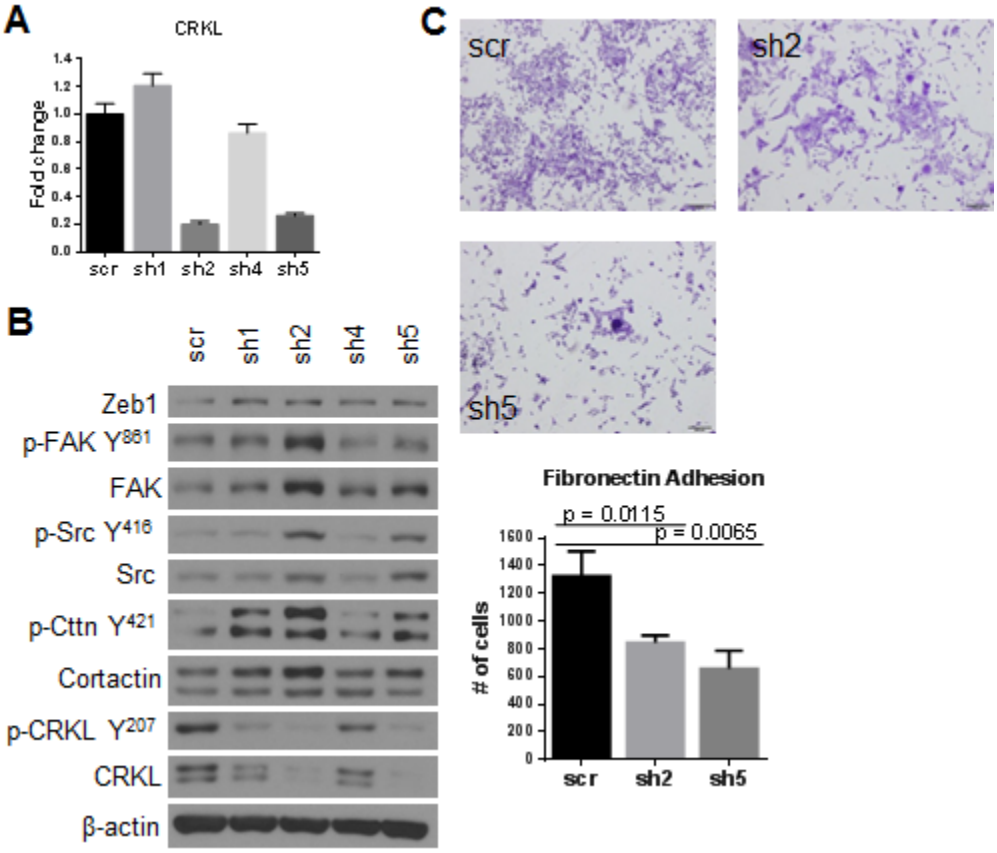

Fig. 37 CRKL knockdown in 393P_ZEB1 cells causes a defect in adhesion. (A) Quantitative RT-PCR and (B) Western Blot analysis of 344SQ cells after CRKL-shRNA knockdown. (C) Adhesion of CRKL shRNA cells on Fibronectin shows a decrease compared to the control cells.

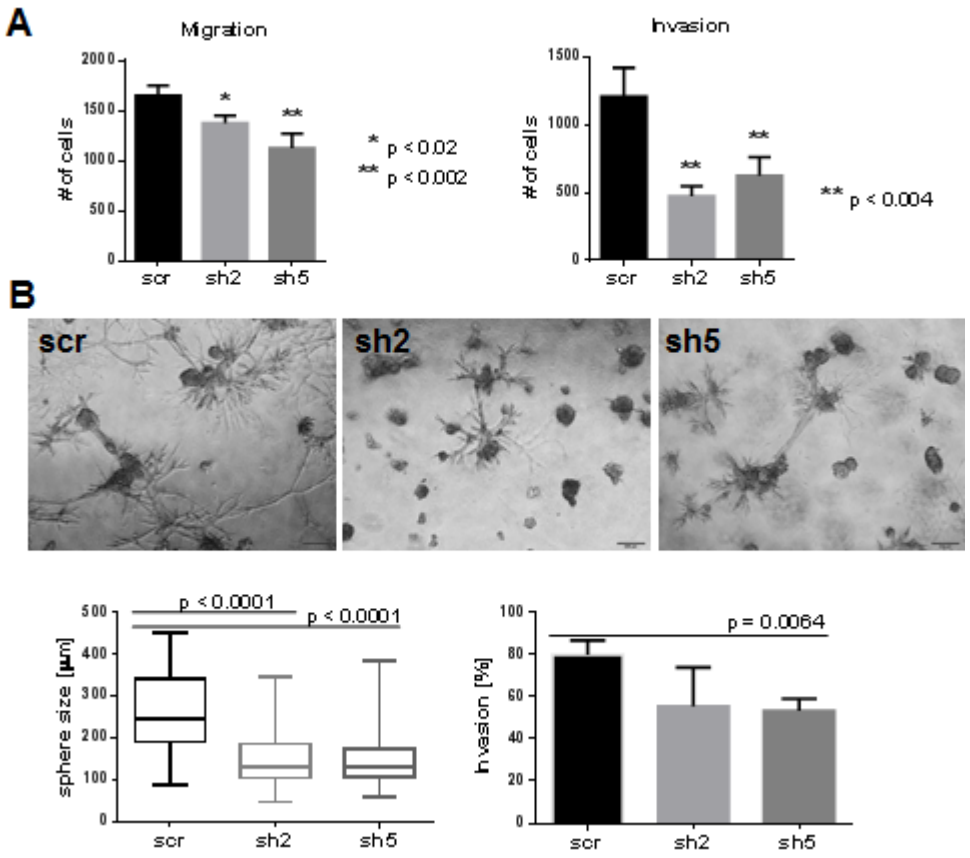

Fig. 38 CRKL knockdown in 393P_ZEB1 cells causes a decrease in migration and invasion. (A) CRKL shRNA causes a significant decrease in Transwell migration and invasion. (B) CRKL knockdown has a slight effect on the 3D invasion in Matrigel/collagen I.

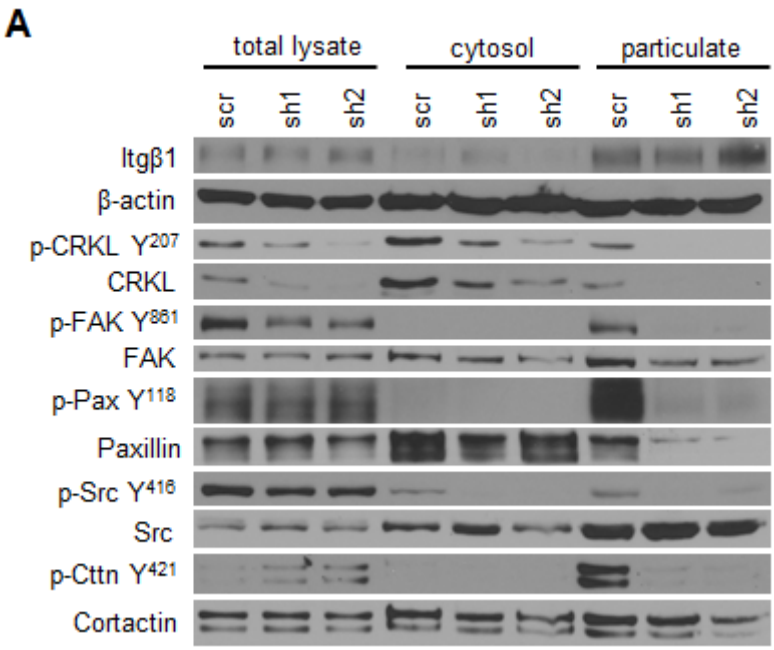

Fig. 39 CRKL knockdown in 344SQ cells causes a decrease of activated FAK and Src localized at the membrane. (A) Cytosol and particulate separation shows a significant decrease in p-FAK, p-Pax, p-Src and p-Cortactin in the particulate fraction compared to the control cells. Itgβ1 is the particulate control, β-actin is the cytosolic control.

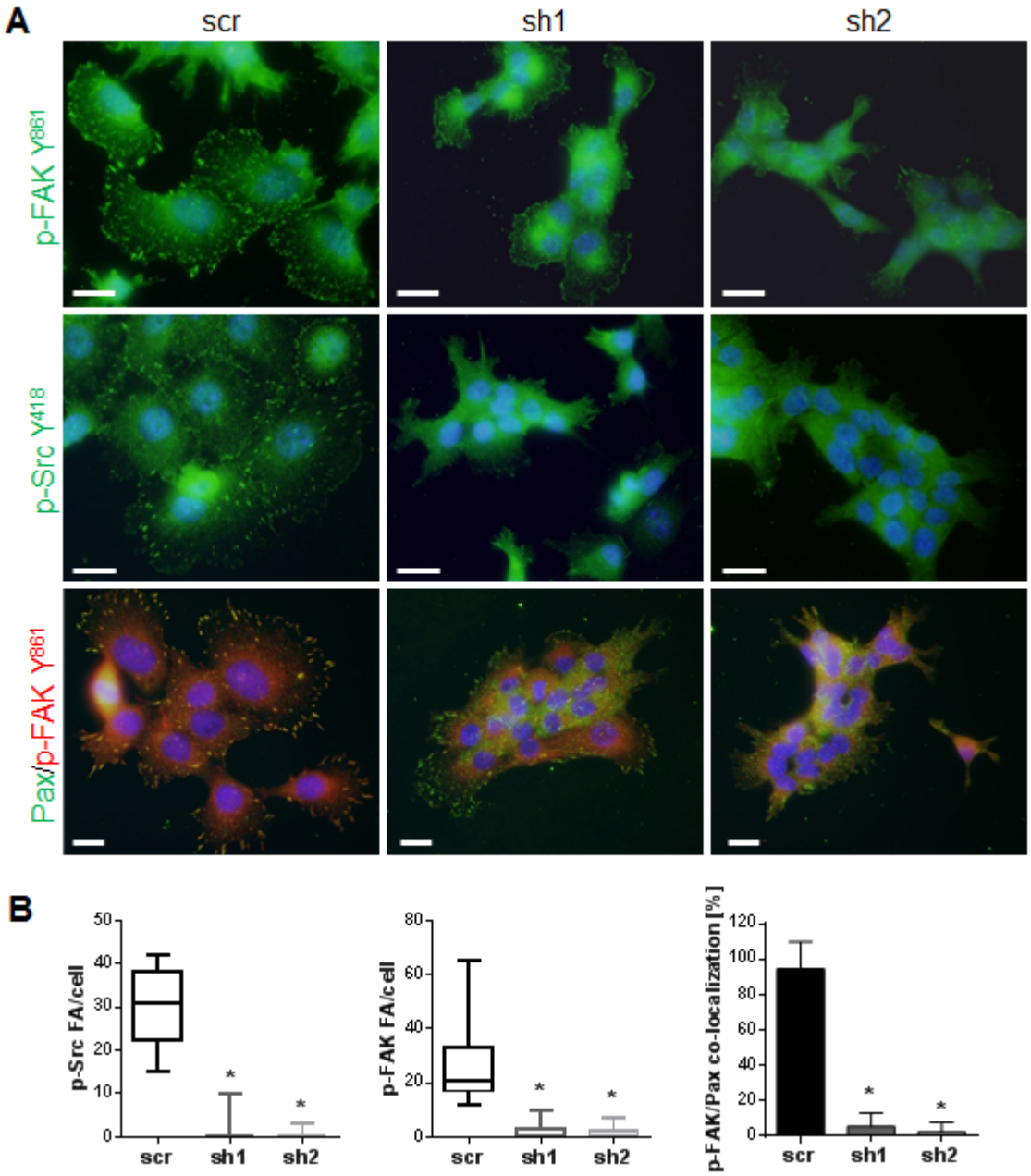

Fig. 40 CRKL knockdown in 344SQ cells affects localization of activated FAK and Src. (A) Immunofluorescent staining for p-Src Y^{418} and p-FAK Y^{861} and co-staining for Paxillin (Pax, for focal adhesions) and p-FAK Y^{861}. Scale bar is 20 µm. (B) Quantification of p-Src and p-FAK at the focal adhesions and co-localization of the focal adhesion marker Paxillin with p-FAK. * $p < 0.0001$

Chapter 4

Discussion

Tumor cell invasion is a complex, multi-step process in which cells acquire a mesenchymal phenotype through changes in the expression of transcription factors and actin associated proteins (including metallo proteinases necessary to degrade the ECM), reorganization of the actin cytoskeleton, as well as changes in the regulation of microRNAs. [7] The acquisition of the mesenchymal phenotype is thought to occur through an epithelial-to-mesenchymal transition, a developmental process which is commonly found in tumor development as well. During the process of EMT cells are reprogrammed to increase their migratory and invasive abilities along with decreased cell-cell adhesion allowing for the enhanced motility. The miR-200/Zeb1 axis, through its double-negative feedback loop, has been well established as a master regulator of EMT. EMT is also induced by changes in signaling pathways (e.g. through mutations) and growth factors such as TGFβ. It is well known that the expression of miR-200 is able to prevent the TGFβ-induced EMT. [7, 10] Despite the knowledge of miR-200 being a master regulator of EMT, the mechanism by how the miR-200/Zeb1 axis regulates the mesenchymal phenotype through alterations of cellular functions remains unclear and was the focus of this study. We used murine cell lines derived from the well-established KP model as well as human lung cancer cell lines to gain a better understanding of the underlying cellular alterations.

In recent years more focus has been on the tumor ECM instead of just the tumor cells since cell-intrinsic changes alone have been shown to be insufficient to drive an invasive phenotype. In our 3D model we confirm those observations by showing that changes in the miR-200 levels alone cells do not become invasive but

hyper-proliferative only when grown in a Matrigel matrix. Similarly, previous studies with our KP model showed that TGFβ-induced EMT or EMT induced by matrix stiffness is insufficient to produce 3D invasion in a synthetic matrix [44]. This study shows that the combination of cell-intrinsic changes and the composition of the ECM, in particular the presence of collagen type I, are necessary to drive tumor cell invasion. In addition to changes in the expression of several cell-surface proteins changes during EMT, it has been shown that the ECM undergoes remodeling during tumor progression [45] . Many of those changes are regulated by microRNAs that target cell adhesion (e.g. cadherins) and ECM (e.g. collagens, fibronectin) molecules [46]. Proteomic and mRNA profiling of cell lines derived from our mouse model showed differences in ECM (collagens, laminins) and adhesion molecules when comparing non-metastatic to metastatic cells [19], suggesting that miR-200 controls both cell-intrinsic changes and changes in the ECM. ECM molecules have been shown to be able to induce an EMT signal, for example through the binding of collagens to integrins leading to the downstream activation of signaling pathways increasing cell motility [8]. The presence of collagen I, found in the ECM surrounding tumors, causes the matrix to become stiffer due to its crosslinking abilities and stiffer matrices have been associated with increased tumor growth and progression (e.g. in breast cancer through modulation of microRNAs) [18] [47]. Our finding that β1-Integrin-collagen I contact is necessary to drive invasion in 3D cultures supports those prior findings and further suggests that the balance cell-cell and cell-matrix interactions driven by miR-200 is crucial for the differential response to the ECM.

This study shows that Zeb1 drives enhanced matrix responsiveness which is due to an increase in the FAK/Src pathway activation, which is significantly decreased in cells with high miR-200 levels. In order to demonstrate the importance of the ECM in regulating intracellular signaling through β1-Integrin-collagen I contact, we utilized 2D and 3D *in vitro* assays in murine and human cells, combined with *in vivo* studies in our well-established KP mouse model to show that the modulation of miR-200 on cell-ECM interactions is applicable in a range of different systems. We further used pharmacological inhibitors and different knock-down approaches *in vitro*, which caused a significant decrease in 2D and 3D invasion, confirming our hypotheses. Previous work has shown that loss of miR-200 drives *in vivo* metastases in our KP model [16], which was significantly decreased upon pharmacological inhibition of Src or knock-down of Itgβ1 as shown in this study. As previously mentioned, the interaction of cells with the ECM is largely dependent on integrins, which further mediate the activation of FAK, yet the exact mechanism of the FAK pathway activation remains to be elucidated. It is known that FAK is phosphorylated and re-localizes to integrin-mediated focal adhesions in stiffer matrices. Once localized at the focal adhesions, it serves as binding partner for Src, which further activates FAK and it can bind multiple adaptor molecules, including Paxillin and p130Cas [18]. Similar to previous studies in which FAK or Itgβ1 siRNA reduced collective cell migration as well as strengthened cell-cell adhesion through E-cadherin modulation, we showed here that FAK or Itgβ1 inhibition, pharmacologically and by shRNA respectively, caused a significant decrease in cell migration and invasion [21].

Due to its important role in EMT, many studies are still trying to understand how miR-200 suppresses EMT, particularly which cellular mechanisms are being regulated. Recent studies have identified that the miR-200 family directly targets multiple actin associated genes, such as moesin, FHOD1, PPM1F, in breast cancer, therefore inhibiting metastasis. [48, 49] A study published this year by Goodall et al. [50] shows a genome-wide screen in breast cancer cells of miR-200 targets which are involved in focal adhesions, invadopodia formation, MMP activity, processes required for tumor cell invasion and characteristics of actin dynamics. We have shown that CRKL, as published in this study, is a direct miR-200 b and c target and functionally effects migration and invasion in lung cancer cells. Our studies have identified that temporary CRKL inhibition using siRNA is necessary for the outside-in integrin-dependent FAK/Src activation as seen by a decreased localization of activated FAK and Src at the focal adhesions. Furthermore, sustained CRKL inhibition using shRNA affects the FAK/Src activation at the biochemical level, leading to decreased 2D and 3D invasion and defects in fibronectin adhesion. In addition, our data suggests that CRKL enhances the inside-out signaling as seen in the FAK and Src inhibitor studies, suggesting a feedback loop between CRKL and the FAK/Src pathway (Fig. 41).

This study highlights the importance of the tumor microenvironment, specifically collagen I, in mediating the activation of intracellular central signaling pathways that drive tumor cell invasion. We have shown that those central pathways can be inhibited at multiple levels, making them attractive targets for new combined treatment strategies in lung cancer patients.

Further studies are needed to identify the effect of CRKL on the FAK/Src complex formation at sites of focal adhesions, its downstream effects on actin reorganization and finally to determine the role of CRKL in *in vivo* metastases, due to its clinical relevance in predicting survival outcome.

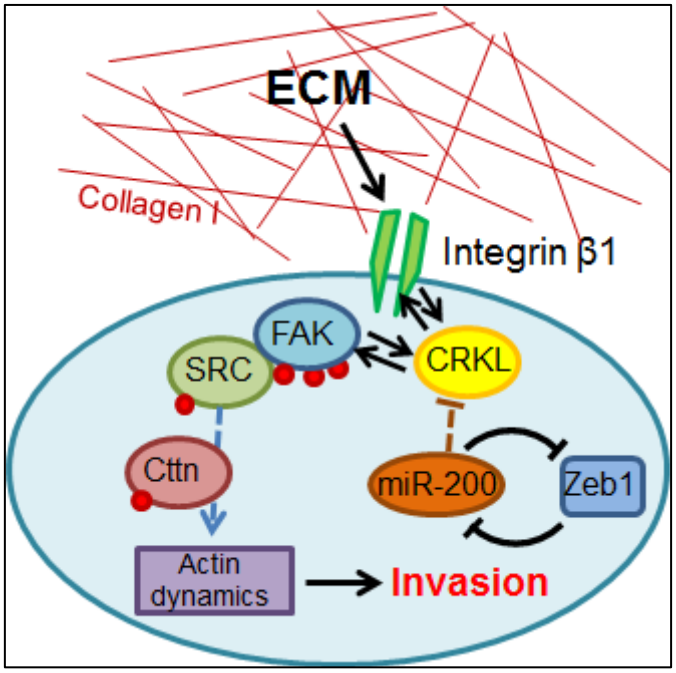

Fig. 41 Proposed model of miR-200/Zeb1 regulating tumor cell activation through β1-integrin-collagen I interaction. Direct targeting of CRKL by miR-200 disrupts the localization and activation of the FAK/Src complex at focal adhesions leading to a decrease in cell migration and invasion.

Bibliography

1. Larsen, J.E. and J.D. Minna, *Molecular biology of lung cancer: clinical implications.* Clin Chest Med, 2011. 32(4): p. 703-40.

2. Siegel, R., J. Ma, Z. Zou, and A. Jemal, *Cancer statistics, 2014.* CA Cancer J Clin, 2014. 64(1): p. 9-29.

3. Gibbons, D.L., W. Lin, C.J. Creighton, S. Zheng, D. Berel, Y. Yang, M.G. Raso, D.D. Liu, Wistuba, II, G. Lozano, and J.M. Kurie, *Expression signatures of metastatic capacity in a genetic mouse model of lung adenocarcinoma.* PLoS One, 2009. 4(4): p. e5401.

4. Zheng, S., A.K. El-Naggar, E.S. Kim, J.M. Kurie, and G. Lozano, *A genetic mouse model for metastatic lung cancer with gender differences in survival.* Oncogene, 2007. 26(48): p. 6896-904.

5. Fidler, I.J., *The pathogenesis of cancer metastasis: the 'seed and soil' hypothesis revisited.* Nat Rev Cancer, 2003. 3(6): p. 453-8.

6. Thompson, E.W. and I. Haviv, *The social aspects of EMT-MET plasticity.* Nat Med, 2011. 17(9): p. 1048-9.

7. Kalluri, R. and R.A. Weinberg, *The basics of epithelial-mesenchymal transition.* J Clin Invest, 2009. 119(6): p. 1420-8.

8. Thiery, J.P., *Epithelial-mesenchymal transitions in tumour progression.* Nat Rev Cancer, 2002. 2(6): p. 442-54.

9. Eger, A., K. Aigner, S. Sonderegger, B. Dampier, S. Oehler, M. Schreiber, G. Berx, A. Cano, H. Beug, and R. Foisner, *DeltaEF1 is a transcriptional repressor of E-cadherin and regulates epithelial plasticity in breast cancer cells.* Oncogene, 2005. 24(14): p. 2375-85.

10. Gregory, P.A., C.P. Bracken, A.G. Bert, and G.J. Goodall, *MicroRNAs as regulators of epithelial-mesenchymal transition.* Cell Cycle, 2008. 7(20): p. 3112-8.

11. Korpal, M., E.S. Lee, G. Hu, and Y. Kang, *The miR-200 family inhibits epithelial-mesenchymal transition and cancer cell migration by direct targeting of E-cadherin transcriptional repressors ZEB1 and ZEB2.* J Biol Chem, 2008. 283(22): p. 14910-4.

12. Korpal, M. and Y. Kang, *The emerging role of miR-200 family of microRNAs in epithelial-mesenchymal transition and cancer metastasis.* RNA Biol, 2008. 5(3): p. 115-9.

13. Bracken, C.P., P.A. Gregory, N. Kolesnikoff, A.G. Bert, J. Wang, M.F. Shannon, and G.J. Goodall, *A double-negative feedback loop between ZEB1-SIP1 and the microRNA-200 family regulates epithelial-mesenchymal transition.* Cancer Res, 2008. 68(19): p. 7846-54.

14. Gregory, P.A., A.G. Bert, E.L. Paterson, S.C. Barry, A. Tsykin, G. Farshid, M.A. Vadas, Y. Khew-Goodall, and G.J. Goodall, *The miR-200 family and miR-205 regulate epithelial to mesenchymal transition by targeting ZEB1 and SIP1.* Nat Cell Biol, 2008. 10(5): p. 593-601.

15. Park, S.M., A.B. Gaur, E. Lengyel, and M.E. Peter, *The miR-200 family determines the epithelial phenotype of cancer cells by targeting the E-cadherin repressors ZEB1 and ZEB2.* Genes Dev, 2008. 22(7): p. 894-907.

16. Gibbons, D.L., W. Lin, C.J. Creighton, Z.H. Rizvi, P.A. Gregory, G.J. Goodall, N. Thilaganathan, L. Du, Y. Zhang, A. Pertsemlidis, and J.M. Kurie, *Contextual extracellular cues promote tumor cell EMT and metastasis by regulating miR-200 family expression.* Genes Dev, 2009. 23(18): p. 2140-51.

17. Seewaldt, V., *ECM stiffness paves the way for tumor cells.* Nat Med, 2014. 20(4): p. 332-3.

18. Keely, P.J., *Mechanisms by which the extracellular matrix and integrin signaling act to regulate the switch between tumor suppression and tumor promotion.* J Mammary Gland Biol Neoplasia, 2011. 16(3): p. 205-19.

19. Schliekelman, M.J., D.L. Gibbons, V.M. Faca, C.J. Creighton, Z.H. Rizvi, Q. Zhang, C.H. Wong, H. Wang, C. Ungewiss, Y.H. Ahn, D.H. Shin, J.M. Kurie, and S.M. Hanash, *Targets of the tumor suppressor miR-200 in regulation of the epithelial-mesenchymal transition in cancer.* Cancer Res, 2011. 71(24): p. 7670-82.

20. Hood, J.D. and D.A. Cheresh, *Role of integrins in cell invasion and migration.* Nat Rev Cancer, 2002. 2(2): p. 91-100.

21. Canel, M., A. Serrels, D. Miller, P. Timpson, B. Serrels, M.C. Frame, and V.G. Brunton, *Quantitative in vivo imaging of the effects of inhibiting integrin signaling via Src and FAK on cancer cell movement: effects on E-cadherin dynamics.* Cancer Res, 2010. 70(22): p. 9413-22.

22. Ganguly, K.K., S. Pal, S. Moulik, and A. Chatterjee, *Integrins and metastasis.* Cell Adh Migr, 2013. 7(3): p. 251-61.

23. Park, C.C., H.J. Zhang, E.S. Yao, C.J. Park, and M.J. Bissell, *Beta1 integrin inhibition dramatically enhances radiotherapy efficacy in human breast cancer xenografts.* Cancer Res, 2008. 68(11): p. 4398-405.

24. Wolfenson, H., Y.I. Henis, B. Geiger, and A.D. Bershadsky, *The heel and toe of the cell's foot: a multifaceted approach for understanding the structure and dynamics of focal adhesions.* Cell Motil Cytoskeleton, 2009. 66(11): p. 1017-29.

25. Mitra, S.K., D.A. Hanson, and D.D. Schlaepfer, *Focal adhesion kinase: in command and control of cell motility.* Nat Rev Mol Cell Biol, 2005. 6(1): p. 56-68.

26. Okada, M., *Regulation of the SRC family kinases by Csk.* Int J Biol Sci, 2012. 8(10): p. 1385-97.

27. Johnson, F.M., B. Saigal, M. Talpaz, and N.J. Donato, *Dasatinib (BMS-354825) tyrosine kinase inhibitor suppresses invasion and induces cell cycle arrest and apoptosis of head and neck squamous cell carcinoma and non-small cell lung cancer cells.* Clin Cancer Res, 2005. 11(19 Pt 1): p. 6924-32.

28. Byers, L.A., B. Sen, B. Saigal, L. Diao, J. Wang, M. Nanjundan, T. Cascone, G.B. Mills, J.V. Heymach, and F.M. Johnson, *Reciprocal regulation of c-Src and STAT3 in non-small cell lung cancer.* Clin Cancer Res, 2009. 15(22): p. 6852-61.

29. Chan, D., J.W. Tyner, W.J. Chng, C. Bi, R. Okamoto, J. Said, B.D. Ngan, G.D. Braunstein, and H.P. Koeffler, *Effect of dasatinib against thyroid cancer cell lines in vitro and a xenograft model in vivo.* Oncol Lett, 2012. 3(4): p. 807-815.

30. Sen, B. and F.M. Johnson, *Regulation of SRC family kinases in human cancers.* J Signal Transduct, 2011. 2011: p. 865819.

31. Zhang, S., W.C. Huang, L. Zhang, C. Zhang, F.J. Lowery, Z. Ding, H. Guo, H. Wang, S. Huang, A.A. Sahin, K.D. Aldape, P.S. Steeg, and D. Yu, *SRC family kinases as novel therapeutic targets to treat breast cancer brain metastases.* Cancer Res, 2013. 73(18): p. 5764-74.

32. Lua, B.L. and B.C. Low, *Cortactin phosphorylation as a switch for actin cytoskeletal network and cell dynamics control.* FEBS Lett, 2005. 579(3): p. 577-85.

33. Cabodi, S., M. del Pilar Camacho-Leal, P. Di Stefano, and P. Defilippi, *Integrin signalling adaptors: not only figurants in the cancer story.* Nat Rev Cancer, 2010. 10(12): p. 858-70.

34. Cheung, H.W., J. Du, J.S. Boehm, F. He, B.A. Weir, X. Wang, M. Butaney, L.V. Sequist, B. Luo, J.A. Engelman, D.E. Root, M. Meyerson, T.R. Golub, P.A. Janne, and W.C. Hahn, *Amplification of CRKL induces transformation and epidermal growth factor receptor inhibitor resistance in human non-small cell lung cancers.* Cancer Discov, 2011. 1(7): p. 608-25.

35. Kobashigawa, Y. and F. Inagaki, *Structural biology: CrkL is not Crk-like.* Nat Chem Biol, 2012. 8(6): p. 504-5.

36. Wang, Y., Q.Z. Dong, L. Fu, M. Stoecker, E. Wang, and E.H. Wang, *Overexpression of CRKL correlates with poor prognosis and cell proliferation in non-small cell lung cancer.* Mol Carcinog, 2013. 52(11): p. 890-9.

37. Senechal, K., C. Heaney, B. Druker, and C.L. Sawyers, *Structural requirements for function of the Crkl adapter protein in fibroblasts and hematopoietic cells.* Mol Cell Biol, 1998. 18(9): p. 5082-90.

38. Kim, Y.H., K.A. Kwei, L. Girard, K. Salari, J. Kao, M. Pacyna-Gengelbach, P. Wang, T. Hernandez-Boussard, A.F. Gazdar, I. Petersen, J.D. Minna, and J.R. Pollack, *Genomic and functional analysis identifies CRKL as an oncogene amplified in lung cancer.* Oncogene, 2010. 29(10): p. 1421-30.

39. La Rosee, P., S. Holm-Eriksen, H. Konig, N. Hartel, T. Ernst, J. Debatin, M.C. Mueller, P. Erben, A. Binckebanck, L. Wunderle, Y. Shou, M. Dugan, R. Hehlmann, O.G. Ottmann, and A. Hochhaus, *Phospho-CRKL monitoring for the assessment of BCR-ABL activity in imatinib-resistant chronic myeloid leukemia or Ph+ acute lymphoblastic leukemia patients treated with nilotinib.* Haematologica, 2008. 93(5): p. 765-9.

40. Li, L., D.L. Guris, M. Okura, and A. Imamoto, *Translocation of CrkL to focal adhesions mediates integrin-induced migration downstream of Src family kinases.* Mol Cell Biol, 2003. 23(8): p. 2883-92.

41. Lee, G.Y., P.A. Kenny, E.H. Lee, and M.J. Bissell, *Three-dimensional culture models of normal and malignant breast epithelial cells.* Nat Methods, 2007. 4(4): p. 359-65.

42. Yang, Y., Y.H. Ahn, D.L. Gibbons, Y. Zang, W. Lin, N. Thilaganathan, C.A. Alvarez, D.C. Moreira, C.J. Creighton, P.A. Gregory, G.J. Goodall, and J.M. Kurie, *The Notch ligand Jagged2 promotes lung adenocarcinoma metastasis through a miR-200-dependent pathway in mice.* J Clin Invest, 2011. 121(4): p. 1373-85.

43. Takayama, Y., S. Tanaka, K. Nagai, and M. Okada, *Adenovirus-mediated overexpression of C-terminal Src kinase (Csk) in type I astrocytes interferes with cell spreading and attachment to fibronectin. Correlation with tyrosine phosphorylations of paxillin and FAK.* J Biol Chem, 1999. 274(4): p. 2291-7.

44. Gill, B.J., D.L. Gibbons, L.C. Roudsari, J.E. Saik, Z.H. Rizvi, J.D. Roybal, J.M. Kurie, and J.L. West, *A synthetic matrix with independently tunable biochemistry and mechanical properties to study epithelial morphogenesis and EMT in a lung adenocarcinoma model.* Cancer Res, 2012. 72(22): p. 6013-23.

45. Thiery, J.P., H. Acloque, R.Y. Huang, and M.A. Nieto, *Epithelial-mesenchymal transitions in development and disease.* Cell, 2009. 139(5): p. 871-90.

46. Valastyan, S. and R.A. Weinberg, *Roles for microRNAs in the regulation of cell adhesion molecules.* J Cell Sci, 2011. 124(Pt 7): p. 999-1006.

47. Mouw, J.K., Y. Yui, L. Damiano, R.O. Bainer, J.N. Lakins, I. Acerbi, G. Ou, A.C. Wijekoon, K.R. Levental, P.M. Gilbert, E.S. Hwang, Y.Y. Chen, and V.M. Weaver, *Tissue mechanics modulate microRNA-dependent PTEN expression to regulate malignant progression.* Nat Med, 2014. 20(4): p. 360-7.

48. Li, X., S. Roslan, C.N. Johnstone, J.A. Wright, C.P. Bracken, M. Anderson, A.G. Bert, L.A. Selth, R.L. Anderson, G.J. Goodall, P.A. Gregory, and Y. Khew-Goodall, *MiR-200 can repress breast cancer metastasis through ZEB1-independent but moesin-dependent pathways.* Oncogene, 2014. 33(31): p. 4077-88.

49. Jurmeister, S., M. Baumann, A. Balwierz, I. Keklikoglou, A. Ward, S. Uhlmann, J.D. Zhang, S. Wiemann, and O. Sahin, *MicroRNA-200c represses migration and invasion of breast cancer cells by targeting actin-regulatory proteins FHOD1 and PPM1F.* Mol Cell Biol, 2012. 32(3): p. 633-51.

50. Bracken, C.P., X. Li, J.A. Wright, D. Lawrence, K.A. Pillman, M. Salmanidis, M.A. Anderson, B.K. Dredge, P.A. Gregory, A. Tsykin, C. Neilsen, D.W. Thomson, A.G. Bert, J.M. Leerberg, A.S. Yap, K.B. Jensen, Y. Khew-Goodall, and G.J. Goodall, *Genome-wide identification of miR-200 targets reveals a regulatory network controlling cell invasion.* EMBO J, 2014.

Vita

Christin Ungewiss was born in Hohenmoelsen, Germany on June 6, 1986, the daughter of Baerbel Queck and Hartmut Queck. After completing her work at Agricolagymnasium, Hohenmoelsen, Germany in 2005, she entered the University of Heidelberg, Germany. She received the degree of Bachelor of Science with a major in molecular biotechnology in July, 2009. From 2009 to 2010 she was enrolled in the Master's Program at the University of Heidelberg, Germany, before entering The University of Texas Graduate School of Biomedical Sciences at Houston in August 2010. She joined Don L. Gibbons' Lab in May 2011.

Permanent address:

2120 El Paseo St Apt 1704
Houston, Texas 77054